Reaction path modelling of *in-situ* mineralisation of CO_2 at the CarbFix site at Hellisheidi, SW-Iceland

Sandra Ó. Snæbjörnsdóttir
Institute of Earth Sciences
University of Iceland
Askja
Sturlugata 7
101 Reykjavík, Iceland
tel. 354-525-5414
fax. 354-525-4499
sos22@hi.is

Reaction path modelling of *in-situ* mineralisation of CO_2 at the CarbFix site at Hellisheidi, SW-Iceland

Sandra Ó. Snæbjörnsdóttir[1], Sigurdur R. Gislason[1], Iwona M. Galeczka[1, 2], Eric H. Oelkers[1, 3, 4]

[1]*Institute of Earth Sciences, University of Iceland, Iceland*

[2] *ISOR, Iceland GeoSurvey, Iceland*

[3]*Earth Science, University College London, UK*

[4]*CNRS/UMR 5563, Université Paul Sabatier, France*

Abstract

Results from injection of 175 tonnes of CO_2 into the basaltic subsurface rocks at the CarbFix site in SW-Iceland in 2012 show almost complete mineralisation of the injected carbon in less than two years (Matter et al., 2016; Snæbjörnsdóttir et al., 2017). Reaction path modelling was performed to illuminate the rate and extent of CO_2-water-rock reactions during and after the injection. The modelling calculations were constrained by the compositions of fluids sampled prior to, during, and after the injection, as reported by Alfredsson et al. (2013) and Snæbjörnsdóttir et al. (2017). The pH of the injected fluid, prior to CO_2 dissolution was ~9.5, whereas the pH of the background waters in the first monitoring well prior to the injections was ~9.4. The pH of the sampled fluids used in the modelling ranged from ~3.7 at the injection well to as high as 8.2 in the first monitoring well. Modelling results suggest that CO_2-rich water-basalt interaction is dominated by crystalline basalt dissolution along a faster, high permeability flow path, but by basaltic glass dissolution along a slower, pervasive flow path through which the bulk of the injected fluid flows. Dissolution of pre-existing calcite at the onset of the injection does not have a net effect on the carbonation, but does contribute to a rapid early pH rise during the injection, and influences which carbonate minerals precipitate. At low pH, Mg, and Fe are preferentially released from crystalline basalts due to the higher dissolution rates of olivine, and to lesser extent pyroxene, compared to plagioclase and glass (Gudbrandsson et al., 2011). This favours the formation of siderite and Fe-Mg carbonates over calcite during

early mineralisation. The model suggests the formation of the following carbonate mineral sequences: siderite at pH <5, Mg-Fe-carbonates and Ca-Mg-Fe-carbonates at pH >5, and calcite at higher pH. Other minerals forming with the carbonates are Al- and Fe-hydroxides, and chalcedony, and zeolites and smectites at elevated pH. The most efficient carbonate formation is when the pH is high enough for formation of carbonates, but not so high that zeolites and smectites start to form, which compete with carbonates over both cations and pore space. The results of reaction path modelling at the CarbFix site in SW-Iceland indicate that this "sweet spot" for mineralisation of CO_2 is at pH from ~5.2-6.5 in basalts at low temperature (20-50°C).

1 Introduction

The reduction of CO_2 emissions to the atmosphere is the one of the biggest scientific challenges of this century (Broecker, 2007; Hoffert et al., 2002; IEA, 2015; IPCC, 2014; Lackner, 2003; Oelkers and Schott, 2005; Pacala and Socolow, 2004). The Paris Agreement (UN, 2015b) aims to keep the global temperature rise "well below 2°C" compared to pre-industrial levels, and to pursue efforts to limit the temperature increase to no more than 1.5 °C. Achieving the goals of the Paris Agreement requires a substantial and sustained reduction in the net flow of CO_2 into the atmosphere. This necessitates the rapid and extensive employment of low-emission technologies and mitigation options (Erbach, 2016; IEA, 2016; OECD/IEA, 2016; UN, 2015a; Yann et al., 2017).

Carbon Capture and Storage (CCS) technologies are expected to play an important role in meeting the Paris Agreement targets. Currently it is the only available technology that can significantly reduce emissions from fossil fuel-based power generation, as well as other industrial processes, such as steel and cement production for the foreseeable future (Global CCS Institute, 2016; IEA, 2016a). The pace of CCS deployment, however, is still far from meeting these challenges (IEA, 2016a; IPCC, 2014). A critical step in CCS is identifying locations and methods for secure subsurface storage of carbon.

The CarbFix project aims at mineralising CO_2 injected into basaltic rocks for its safe and long-term storage. The injection of CO_2 into basaltic rocks offers several advantages over more conventional storage including its ability to promote rapid mineralisation and its large potential storage volume (Gislason and Oelkers, 2014; Goldberg and Slagle, 2009; McGrail et al., 2006; Snæbjörnsdóttir et al., 2014). In the CarbFix method, CO_2 is dissolved in water prior to, or during its injection into porous basalts (e.g. Gislason and Oelkers, 2014; Sigfusson et al., 2015, Matter et al., 2016). Basaltic rocks are rich in divalent cations such as Ca^{2+}, Mg^{2+}, and Fe^{2+}. Once dissolved, the CO_2 is no longer buoyant, and the acidic CO_2-charged fluid accelerates the release of these metals through basalt dissolution, promoting the formation of carbonate minerals including calcite, magnesite, siderite, and carbonate solid-solutions (Gislason et al., 2014; Gislason and Oelkers, 2014), thereby providing mineral storage of the injected CO_2.

This paper follows three previous reports on the CarbFix injections: 1) a detailed description of the injection method and data from the injection well was provided by Sigfusson (2015); 2) the monitoring of chemical tracers, dissolved inorganic carbon, and pH in the first monitoring well downstream from the injection well was reported by Matter et al. (2016); and 3) the concentrations of dissolved major elements during and after injection in the first monitoring well, as well as the saturation indices of potential secondary minerals were described by Snæbjörnsdóttir et al. (2017). Here we use fluid composition data collected prior to, during, and after the injection of 175 tonnes of pure CO_2 into the subsurface basaltic rocks at the CarbFix site in SW-Iceland to model CO_2-water-rock interaction during and after the injection. Modelling results will be used to illuminate the fate of the CO_2 following its injection, and gain insight into the processes that occur between the basaltic bedrock, the injected fluids, and the pre-existing formation waters. In addition to the improved understanding of CO_2-water-basalt interaction during the mineral storage of CO_2, these modelling results also provide new insights into water-basalt interaction during natural, shallow depth, and elevated pCO_2 processes (e.g. Neuhoff et al., 2006).

2 Methods

2.1 Site description

The CarbFix injection site has been described in detail in several papers (Alfredsson et al., 2013; Aradóttir et al., 2012; Snæbjörnsdóttir et al., 2017). The site is located in SW-Iceland, about 30 km east of Reykjavík, and about 3 km SW of the Hellisheidi geothermal power plant, which is owned and operated by Reykjavik Energy. The power plant annually produces about 40,000 tonnes CO_2 and 12,000 tonnes of H_2S as a by-product of geothermal energy production. The gases are of magmatic origin.

In January to March 2012, 175 tonnes of pure CO_2 were dissolved into co-injected water as it descended into well HN-02, a 2001 m deep injection well located at the site (Fig. 1), as described in detail by Sigfusson et al. (2015). Carbon-14 (^{14}C), a reactive tracer, and sulphur hexafluoride (SF_6), a non-reactive tracer were co-injected with the CO_2-charged water. The injection site is equipped with eight monitoring wells that penetrate the groundwater system affected by the injection. The pH of the formation water in the monitoring wells penetrating the target groundwater system was 8.9-9.9 prior to the injection (Alfredsson et al., 2013). Extensive monitoring was carried out prior to, during, and after the injection via sampling of the first monitoring well, HN-04. At the surface the distance between HN-04 and the injection well, HN-02, is 10 m, but due to the subsurface diversion of HN-04, the distance between the wells is ~125 m at 520 m depth, where the target carbon storage aquifer is located (Alfredsson et al., 2013; Aradóttir et al., 2012; Fig. 1).

The storage formation consists of basaltic lavas of olivine tholeiitic composition, as described in detail by Alfredsson et al. (2013) and Helgadóttir (2011). The lava flows are characterized by crystalline interiors, and glassy scoria-rich tops and bases formed due to more rapid cooling. Fractures and faults are common in the area, which is tectonically active, as it is located on a triple junction where two active rift zones meet a seismically active transform zone (Foulger, 1988). The initial rock porosity ranges from 5 to 40% (Franzson et al., 2008) and is mostly present at the glassy boundaries of these flows, but

also in cooling cracks columnar jointing, younger fractures, and tectonic faults (e.g. Alfredsson et al. 2013). The major pre-existing alteration phases at the depth of the CO_2 injection, at about 500 m and 30-50°C, are pore filling Ca–Mg–Fe–smectites, Ca-rich zeolites, chalcedony, and calcite; these phases are typically found in vesicles and fractures of the primary rocks (Alfredsson et al., 2013; Helgadóttir, 2011; Table 1). These phases are characteristic of low temperature basaltic rock alteration (Kristmannsdóttir and Tómasson, 1978), and reflect the low partial pressure of CO_2 ($>10^{-2}$ bar) and high pH (>9) of the groundwater of the storage formation. Smectite-zeolite alteration can lead up to a 40% decrease in the initial porosity (Neuhoff et al., 2008).

Field tracer tests were conducted during 2008-2011, both under natural and forced flow conditions to define the system hydrology. Hydrological modelling (Khalilabad et al., 2008), and later reactive transport models (Aradóttir et al., 2012) were used to define the system hydrology and to characterize the flow between the injection well HN-02, and the first monitoring well, HN-04 (Khalibad et al. 2008). Most of the storage formation consists of relatively homogenous porous media flow with considerable dispersion and diffusion, with effective matrix porosity of 8.5%, but a fast breakthrough path, most likely caused by fracture or a thin interlayer connecting the wells, was found to channel about 3% of the flow between wells HN-02 and HN-04 (Aradóttir et al., 2012; Khalilabad et al., 2008). The lateral and vertical intrinsic permeabilities were estimated to be 300 and 1700×10^{-15} m^2, respectively, and the regional undisturbed groundwater flow velocity was estimated to be about 25 m y^{-1} (Aradóttir et al., 2012). The groundwater flow between the wells was accelerated during the injection and the subsequent monitoring period by pumping water into the HN-02 injection well at 2 kg s^{-1} and by producing water at 1 kg s^{-1} from the first monitoring well (HN-04). Both wells were sampled regularly prior to, during, and after the injection. The sampling procedure is described in detail by Snæbjörnsdóttir et al. (2017).

2.2 Geochemical modelling

Reaction path modelling was performed to illuminate the identity and extent of fluid-mineral reactions during and after the first CarbFix injection at Helisheidi, in January to

March 2012. Efforts were made to model the reaction path of the first breakthrough of the injected CO_2-rich fluid, which channelled about 3% of the injected fluid and arrived at the first monitoring well (HN-04) about 60 days after the onset of the injection, and the second breakthrough of the bulk of the injected fluid, arriving about 400 days after the onset (Fig. 2).

The geochemical reactions were studied as a function of the mass of basalt dissolved into the CO_2-charged injection fluid, both in terms of secondary mineral formation and water chemistry. Aqueous speciation, mineral saturation states, and reaction path calculations were performed using PHREEQC (Parkhurst and Appelo, 2013). The standard PHREEQC database was used in all calculations after including revised thermodynamic data for the primary and secondary minerals of basaltic rocks and basaltic rock alteration taken from Gysi and Stefánsson (2011, Table 2). The calculations were performed assuming that the oxygen fugacity was controlled by equilibrium with the Fe^{2+}/Fe^{3+} redox couple. The measured pH of sampled monitoring well fluids, representing the two breakthroughs, was used as a guideline in the modelling. The aim was to produce fluids with similar chemical composition to those sampled during the breakthroughs. The mass and volume of dissolved and precipitated phases and the chemical compositions of the precipitating phases were calculated.

Three processes have been identified to account for the chemical evolution of the injected fluids sampled from the HN-04 monitoring well (Matter et al., 2016; Snæbjörnsdóttir et al., 2017):

1) The mixing of the acidic injection fluids with the alkaline formation waters.
2) The dissolution of the pre-existing glasses and minerals of the storage host primary basalt during and after the injection.
3) The dissolution of pre-existing calcite within the storage formation at the onset of the injection.

The mixing of the injection fluid with the background waters is most certainly a gradual process, which starts as soon as the injected fluid enters the storage formation and continues until this fluid enters the monitoring wells. While the conservative chemical

tracers provide a quantitative mixing ratio between the injected fluid and formation waters in samples collected from the first monitoring well, field observations provide little insight into the temporal evolution of this mixing process. As such, we performed initial modelling calculations assuming either 1) the injected CO_2-charged injection fluid mixed with the formation water immediately upon entering the subsurface followed by basalt dissolution; 2) the dissolution of basalt and calcite into the injected fluids was followed by its mixing with formation water; or 3) the continuous mixing of the injected fluid with the formation fluids as basalt dissolved. Comparison of these modelling results with field observations showed a best fit with the second model. As such all calculations below were performed assuming the injected fluid first reacted with the basalt and then was diluted by mixing this reacted fluid with formation water in the proportions prescribed by the measured conservative tracers.

2.2.1 The fluid phases

A representative composition of the formation waters, prior to the arrival of the CO_2-rich injected fluids, was sampled from the first monitoring well (HN-04) on the 25th of January 2012. The chemical composition of this water sample, 12KGM01, was previously reported by Snæbjörnsdóttir et al. (2017) and is provided in Table 3. Similarly, the composition of the injection fluid prior to the addition of dissolved CO_2 and chemical tracers is represented by sample 12KGM06, collected from well HN-01 on the 3rd of February 2012. This chemical composition was previously reported by Snæbjörnsdóttir et al. (2017) and is provided in Table 3. Water was first pumped from well HN-01, as shown in Fig. 1. The CO_2 gas and tracers were dissolved into this water during its injection into the subsurface as described by Sigfusson et al. (2014). The CO_2-charged water was then released into the basaltic storage formation at a depth of ~520 m and a temperature of about 35°C (Fig. 1). The dissolved inorganic carbon (DIC) concentration of this water as it enters the storage formation was 0.82 mol/kg on average. After its injection into the subsurface, this water is affected by both fluid-mineral interaction with the subsurface rocks, and dilution via mixing with the pre-existing formation waters.

The fluids continuously produced out of the first monitoring well, HN-04, were regularly sampled during the injection and over the subsequent months. The samples consist of a mixture of the injected fluid and the formation fluids. The mixing fraction of these two fluids was calculated using the non-reactive SF_6 tracer concentration and mass balance calculations by Matter et al. (2016). Two samples collected during the arrival of the major parts of the CO_2-rich water plume to the first monitoring well are sample 12KGM33, collected about 60 days after the onset of the injection, and sample 13SOS06, collected about 400 days after the onset of the injection. These samples are representative of the chemical compositions of the subsurface fluids during the first and second plume breakthroughs (Fig.2). The chemical compositions of these samples are provided in Table 3, and were previously reported by Snæbjörnsdóttir et al. (2017).

2.2.2 Host rock reactivity

The subsurface storage formation at the CarbFix site consists mainly of a combination of glassy and crystalline basalts with some secondary phases as described in section 2.1. The interaction between the basaltic rock and the CO_2-charged acidic injection fluid can be viewed as a titration process, where the basaltic rocks act like a base which titrates into aqueous carbonic acid, consuming protons and releasing cations upon dissolution (Table 2). This raises the fluid pH to a range favouring carbonate precipitation when some of the released cations combine with the injected CO_2 to form stable carbonate minerals.

The composition of the glassy basalts at the injection site is close to that of the Stapafell Mountain located in SW–Iceland, near the CarbFix injection site. Its chemical composition, normalised to one Si atom, is consistent with $SiTi_{0.024}Al_{0.358}Fe_{0.188}Mg_{0.281}Ca_{0.264}Na_{0.079}K_{0.008}O_{3.370}$ (e.g. Gysi and Stefánsson, 2011; Oelkers and Gislason, 2001) and its molar weight, based on its Si normalized composition, is 123 g/mol. The reactivity of the Stapafell basaltic glass has been extensively studied (Galeczka et al., 2014; Gislason and Oelkers, 2003; Oelkers and Gislason, 2001; Stockmann et al., 2011; Wolff-Boenisch et al., 2004). The dissolution of basaltic glass is considered to include two basic steps: 1) non-stoichiometric dissolution due to a formation of a leached layer,

where alkali and alkaline-earth metals are preferentially removed, followed by 2) the steady-state, stoichiometric dissolution of the Al and Si enriched leached layer (Oelkers and Gislason, 2001). The dissolution of this Al- and Si-rich surface layer is the rate-limiting step of the dissolution (e.g. Gislason and Oelkers, 2003; Guy and Schott, 1989). The chemical composition of Stapafell basaltic glass and its reactivity is used in the model calculations as described below.

The crystalline basalts consist of olivine, pyroxene, plagioclase, and to a lesser extent iron oxides and glass. More than 90% of the crystalline fraction of the CarbFix subsurface storage consists of plagioclase (plag), pyroxene (pyr) and olivine (ol). The dissolution rates of crystalline basalt were measured and reported by Gudbrandsson et al. (2011). These rates were originally modelled by these authors assuming the basalt consists of only the three major phases, plag: pyr: ol with modal abundances of 44:39:17. To be consistent with these experimental results, the equations and relative mineral surface areas of Gudbrandsson et al. (2011) were adopted in this study. Note that the contribution of glass and iron oxides to the elemental fluxes are considered negligible in the Gudbrandsson et al. (2011) model. Thermodynamic properties of the phases of the minerals present in crystalline basalts used in the modelling were taken from Gysi and Stefánsson (2011) – see Table 1.

In addition to the dissolution of the primary rocks in the storage formation, some dissolution of pre-existing secondary phases likely occurred. This applies particularly to calcite, due to its rapid dissolution kinetics. Matter et al. (2016) measured the $^{14}C/^{12}C$ ratio of samples collected from the first monitoring well, suggesting a ~50% dilution of the injected fluid ^{14}C during the first breakthrough, and a ~10% dilution of the injected fluid ^{14}C during the second breakthrough, most likely via dissolution of pre-existing calcite shortly after the injection of the CO_2-charged fluid into the basaltic storage formation. The effect of the carbonate dissolution on the system evolution is discussed in section 4.3.

2.2.2.1 The fast-flow path of the first breakthrough

This first breakthrough path is characterized by a relatively fast flow between the injection well and the first monitoring well, channelling ~3% of the injected fluid (Khalilabad et al., 2008). The pH was measured to be as low as 6.7 in the sampled monitoring fluids during the first breakthrough.

Crystalline basalt was selected to represent the dissolving primary rock of the first breakthrough for two reasons:

1) Preliminary modelling calculations of the first breakthrough using basaltic glass as the main dissolving phase results in fluids having compositions inconsistent with those sampled from this first breakthrough; notably computed Na and DIC were substantially higher than their measured counterparts. This difference could be explained by the faster release rates of divalent cations from crystalline basalts compared with basaltic glass. Notably at acid to neutral conditions, Mg and Fe are preferentially released from crystalline compared to glassy basalts due to the higher dissolution rates of olivine, and to lesser extent pyroxene, compared to plagioclase and glass (Gudbrandsson et al., 2011).
2) This is further supported by the aquifer characterisation reported by Khalilabad et al. (2008), indicating the first breakthrough to be associated with a shallow depth fracture flow between the two wells at. The depth of the aquifer in the injection well HN-02 is at about ~550 m, but the depth of the fracture pathway channelling the first breakthrough to well HN-04 is at about ~420 m. This indicates fracturing through the interiors of the lava-pile, likely transecting the crystalline surfaces of the bedrock.

Taking these observations into account, the primary crystalline rock and calcite was dissolved into the CO_2-charged injection fluid, and later mixed with the background waters in the model calculations, as described in Fig. 3.

2.2.2.2 The second breakthrough flow-path of the bulk of the injected fluid

This second breakthrough path is hosted within a large volume of homogenous media with inter-connected porosity, channelling the bulk of the injected fluid (Khalilabad et al., 2008). The pH of the sampled fluids collected from the first monitoring well during this second breakthrough was measured to be ~8.2. The fluid composition evolution along this slow flow path is likely to be dominated by basaltic glass dissolution; basaltic glass dominates the tops and bases of individual lava flows of the olivine-tholeiite lava pile in the storage formation (e.g. Alfredsson et al., 2013) and hosts the main flow paths of fresh to moderately altered lava pile (e.g. Franzson, 2000; Neuhoff et al., 2008). Preliminary modelling calculations of the second breakthrough showed a relatively good fit with the sampled fluids compositions when assuming basaltic glass dissolution dominated fluid-rock interaction. Within the model calculations of the second breakthrough, therefore, basaltic glass was dissolved into the CO_2-charged injection fluid along with calcite, and later mixed with the background waters, as described in Fig. 3.

2.2.3 The precipitating phases

The chemical compositions of the secondary phases that were allowed to precipitate during the reaction path modelling, if they became saturated in the aqueous phase, are provided in Table 2. These secondary phases are consistent with those found during the low temperature (<100°C) alteration of Icelandic basaltic rocks, as well as those carbonate minerals that potentially form at low temperatures and elevated CO_2-pressures from the release of Ca, Mg, and Fe, as reported by Rogers et al. (2006), and Gysi and Stefánsson (2011). The choice of these secondary minerals is further justified by field observations of natural processes (e.g. Alfredsson et al., 2013; Kristmannsdóttir and Tómasson, 1978; Neuhoff et al., 1999), laboratory observations of low temperature CO_2-water-basalt interaction (Gysi and Stefánsson, 2012), and from results of CO_2 field injection experiments (Matter et al., 2016; Snæbjörnsdóttir et al., 2017).

The saturation states of Al-hydroxides, zeolites, and clays depend strongly both on the chemical composition and thermodynamic data chosen for each phase. The zeolites taken into account in this study are those observed in drill cuttings collected from the injection

well (Alfredsson et al., 2013) and those known to be stable at temperatures below 75°C (Helgadóttir, 2011; Kristmannsdóttir and Tómasson, 1978). The clay minerals considered are smectites with a chemical composition similar to that reported from the area of the injection (Schiffman and Fridleifsson, 1991; Snæbjörnsdóttir, 2011). Due to the low pH, low temperature, and the short residence time of CO_2-water-rock interaction, clay minerals and zeolites were excluded in the modelling of the first breakthrough due to their sluggish precipitation rates (e.g. Kloprogge et al., 1999; Neuhoff et al., 2000).

3 Results

3.1 The computed fluid compositions in the absence of basalt-fluid interaction

The initial pH of the injected fluid, prior to injection and CO_2 dissolution, was measured to be ~9.5. The CO_2 was then dissolved into this fluid, leading to a dissolved carbon concentration of 0.82 moles per kg of water. Fluid speciation calculations indicate that the pH of the resulting fluid was 3.7 at 35°C. The chemical composition of this CO_2-rich injection fluid, as represented by sample 12KGM06, is shown in Table 3. The only saturated phase in this CO_2-charged fluid was chalcedony; all carbonate minerals were highly undersaturated (Table 4).

The pH of the monitoring well fluids at the onset of the injection was measured to be 9.2, as represented by sample 12KGM01 (Table 3). The saturated phases in the fluid were smectites, zeolites, calcite, and aragonite (Table 4). The pH of the fluids sampled from the first and second injection fluid breakthroughs at the first monitoring well was measured to be 6.7 and 8.2 respectively, as represented by samples 12KGM33, and 13SOS06 (Table 3). This high pH relative to the injection fluid indicates significant water-CO_2-rock interaction with the subsurface storage formation, and mixing with the alkaline background waters along the flow-paths between the injection well and the first monitoring well.

The fraction of alkaline formation fluids mixed into the acidic injection fluid in the subsurface was calculated using the SF_6 non-reactive tracer together with non-reactive,

conservative fluid mixing calculations, as described by Matter et al. (2016). The effect of this fluid mixing in the absence of fluid-basalt interaction are shown in Fig. 4. The pH increase resulting from mixing of the two fluids accounts for a pH rise from 3.7 to 4.6 during the first breakthrough with a 90% mixing fraction of the alkaline formation waters (Fig. 2-3), and from 3.7 to 4.1 during the second breakthrough of the injected solution breakthrough with a 60% mixing fraction of the alkaline formation waters. Chalcedony is the only saturated phase in both fluid mixtures, as was the case for the CO_2-charged injection fluid (Table 4). All carbonate minerals are highly undersaturated.

3.2 The first breakthrough

The first breakthrough resulting from the arrival of ~3% of the injected CO_2-charged water occurred in well HN-04 about 60 days after the onset of the injection, as indicated by the SF_6 non-reactive tracer concentrations in the monitoring well fluid samples (Matter et al. 2016, Fig. 2). The pH of the fluids collected from the monitoring well of this first breakthrough was about 6.7 and the DIC concentration was 4.0 mmol/L (Snæbjörnsdóttir et al., 2017; Table 3). Pure mechanical mixing of the injected CO_2-charged water with the formation waters, using the observed 1:9 ratio in the sample, would result in pH 4.6 and DIC concentration of 88 mmol/L (as described in section 3.1; see Fig 6), indicating the significance of mineral fluid reaction.

The best match between the modelled results and field observations was obtained when 0.42 moles/kg of the crystalline rock (~64 g); in total 0.36 moles kg^{-1} olivine, 0.05 moles kg^{-1} clinopyroxene, and 0.01 moles kg^{-1} plagioclase, were calculated to have dissolved into each kilo of the injected CO_2-charged fluid, taking into account the relative dissolution rates of these minerals in crystalline basalt reported by Gudbrandsson et al. (2011). The primary rock was dissolved into the CO_2-charged injection fluid together with 0.82 moles kg^{-1} (82 g) of calcite. The quantity of calcite dissolution was estimated from the $^{14}C/^{12}C$ ratio of the monitoring well fluids suggesting ~50% dilution (see section 2.2.2 and Matter et al., 2016).

The results of the reaction path simulations are shown in Fig. 5, including the pH, pCO_2, and secondary phase mineralogy as a function of time. A comparison of the chemistry of fluids sampled from the HN-04 monitoring well (Table 3) during the first breakthrough with those computed in this study are shown in Fig. 6. Chalcedony is calculated to be the first alteration phase to form, together with minor amounts of Fe- and Al-hydroxides (e.g. microcrystalline gibbsite) (Fig 5.d-e). The first carbonate-phase calculated to form is siderite ($FeCO_3$) at pH ~5 (Fig. 5 a-c). Note that the formation of carbonates at such low pH is favoured by the high pCO_2 of the injected fluid. Gradually, the carbonates become more Mg-, and Ca-rich, with the formation of $Mg_{.25}Fe_{0.75}$-solid solution, and subsequently a $Ca_{0.25}Mg_{0.50}Fe_{0.25}$-solid solution, and calcite (Fig. 5b-c).

3.3 The second breakthrough

The second breakthrough occurring as the peak concentration of the SF_6-non reactive tracer arrived at the HN-04 monitoring well, indicating the arrival of the bulk of the injected fluid, occurred about 400 days after the onset of the injection (Matter et al., 2016; Fig. 2). A slight drop in pH, together with a slight increase in DIC, was noted in the fluid samples collected from HN-04 during this breakthrough. The pH of this second breakthrough was measured to be about 8.2 and the DIC concentration about 3 mmol/L (Table 3). Pure mechanical mixing of the injected fluid with a 3:2 ratio of the formation fluids would result in pH of 4.1 and DIC concentration of about 350 mmol/L (Fig. 6). This indicates that the bulk of the injected carbon was mineralised along the flow-path towards the monitoring well within 400 days after the onset of the injection, as previously reported by Matter et al. (2016) and Snæbjörnsdóttir et al. (2017). This is also supported by ^{14}C-data as described by Matter et al. (2016), and the net-input of Ca, Mg, and Fe via host rock dissolution as described by Snæbjörnsdóttir et al. (2017).

The results of the reaction path calculations are shown in Fig. 6 and 7, including the fluid composition, pH, and pCO_2, and secondary phase mineralogy, as a function of time. The best match between the modelling results and the chemical compositions of the sampled monitoring well fluid at the second breakthrough, requires the dissolution of 0.86 moles of

basaltic glass (~106 g) into each kg of the injected CO_2-charged water. The basaltic glass was dissolved into the injection fluid, along with 0.082 moles kg^{-1} (8.2 g) of calcite, estimated from the $^{14}C/^{12}C$ ratio of the monitoring well fluids suggesting a ~10% dilution of the injected carbon with carbonate from calcite dissolution (see section 2.2.2 and Matter et al., 2016). This fluid was then mixed with the formation waters, based on the mixing fraction calculated by the SF_6 tracer. The resulting modelling results are in close agreement with the sampled fluid during the second breakthrough of the injected fluid in the monitoring well HN-04, as shown in Fig. 6b.

The modelling calculations suggest that the first minerals to precipitate from the injected CO_2-charged fluid, at high pCO_2 and pH <6.5, are aluminium hydroxides (microcrystalline gibbsite) and chalcedony, with some minor iron-hydroxides (Fig.7d-e). Carbonate minerals begin to form at around pH 5. Again, the low pH of the initial carbonate mineral formation is due to the high pCO_2 of the fluid phase. The first carbonate-phase predicted to form is siderite at pH ~5. As the fluid evolves above pH 5, the carbonates become more Mg-rich and Ca-rich, with the formation of a $Ca_{0.25}Mg_{0.25}Fe_{0.50}$-solid solution, followed by a $Ca_{0.25}Mg_{0.50}Fe_{0.25}$-solid solution, and lastly calcite (Fig.7b-c). Calcite is the dominant carbonate forming when the pH reaches ~8. At pH ~6.9 the zeolite analcime is calculated to start forming, and thomsonite at pH ~7.6. Finally, smectite is calculated to become supersaturated at pH ~8.0, and Mg-clays at pH ~8.1 (Fig.7d-e).

4 Discussion

4.1 Mineral sequences – comparison to experiments and natural analogues of basalt-CO_2 interactions

The results of the reaction path modelling described above indicate the formation of mineral sequences in agreement with observed secondary mineralogy, formed by the alteration of basaltic rocks in natural systems with high pCO_2 and temperatures below 100°C (Rogers et al., 2006), and during CO_2-water-basalt experiments (Gysi and Stefánsson, 2012). The results of the reaction path modelling are also in good agreement with the computed saturation states of the sampled fluids during and after the injection

(Snæbjörnsdóttir et al., 2017), and the reaction path modelling of CO_2-water-basalt interaction at 25°C reported by Gysi and Stefánsson (2011).

The chemical composition of the carbonates formed is influenced by the mobility of divalent cations, mainly Ca, Mg, and Fe. Speciation calculations indicate that all carbonates are undersaturated in the acidic injection fluid, and in the absence of water-CO_2-basalt interaction (e.g. in the pure mixing calculations presented in section 3.1). In contrast, due to water-CO_2-basalt interaction, as the pH reaches ~5, Fe^{2+}-carbonates such as siderite and Fe rich Mg-Fe and Ca-Mg-Fe-solid solutions are calculated to form. The formation of such iron-rich carbonates is highly dependent on the fluid oxidation state and the availability of Fe^{2+} dissolved from the primary rock. The Fe^{2+}-rich carbonates dominate carbonate precipitation at pH <5.5; while at higher pH the Fe^{2+} oxidation becomes more important leading to the formation of Fe^{3+} bearing clays and Fe-oxides, along with more Mg- and Ca-rich carbonates. This is in agreement with calculated saturation states of the first monitoring well fluids during the first breakthrough, as reported by Snæbjörnsdóttir et al. (2017); and the results of the modelling of CO_2-basalt interaction reported by Gysi and Stefánsson (2011).

The formation of Fe-rich carbonates is also favoured by the fast dissolution rates of Fe-bearing olivine and pyroxene in crystalline basalts, as described by Gudbrandsson et al. (2011). Siderite has not been identified at the field site, but was identified as a product of basalt-CO_2-water interaction in Greenland, along with Fe-Mg and Fe-Ca-Mg-carbonate solid solutions (Rogers et al., 2006). These carbonates have also been identified in drill-cuttings from the Svartsengi geothermal field in SW-Iceland (Richter et al., 1999), which has a significantly higher salinity and higher temperature gradient than the CarbFix site.

Progressive basaltic rock-dissolution provokes an increase in pH and a decrease in dissolved CO_2 concentration through the formation of Ca-rich carbonates, such as calcite, and Ca-Mg-Fe-solid solutions. At higher pH, carbonates become more abundant, forming along with chalcedony, and later both zeolites, and smectites (Fig. 7b-e). Speciation calculations of the fluids sampled during the second breakthrough show that they are

saturated with respect to siderite, Ca-Mg-Fe-solid solutions, and calcite, as well as smectites and zeolites (Snæbjörnsdóttir et al., 2017). This is also in agreement in with the modelling reported by Gysi and Stefánsson (2011), which shows increased mass of secondary minerals forming with the increasing basalt dissolution.

As previously mentioned, calcite and aragonite are the only carbonate phases identified to be present in the formation rocks prior to the injections (Alfredsson et al., 2013). Furthermore, calcite was the only carbonate phase identified on the precipitates forming on the submersible pump in the monitoring well HN-04 in the months after the second breakthrough, along with some trace amounts of clays (Snæbjörnsdóttir et al., 2017). This is in agreement with the reaction path calculations at pH >8, where the only carbonate phase precipitating is calcite, along with smectites and zeolites (Fig.7b-c). This is also in agreement with the modelling work of Gysi and Stefánsson (2011), which shows the reduced mobility of Al, Si, Mg and Fe at alkaline conditions due to smectite and zeolite formation. These observations, however, do not exclude the formation of Fe-rich carbonates during and after the injection. The precipitation of Fe-bearing carbonate minerals at pH <6 could either have formed in the subsurface closer to the injection well, and/or were dissolved when pH increased, and re-precipitated as more stable carbonates such as calcite.

4.2 The efficiency of carbon mineralisation in basaltic rocks

Two key factors are essential for successful mineral storage of CO_2 in basaltic rocks:

1) Sufficient permeability and/or active porosity, providing flow paths for efficient injection of the CO_2-rich fluid, and mineral surfaces for geochemical reactions to occur, and
2) conditions favourable for the efficient formation of carbonate minerals.

The CO_2-water-rock interaction between the injected fluid and the basaltic rocks results in the formation of secondary phases with significant volume and porosity changes (Fig. 5c

and e, Fig. 7c and e, Fig. 8). The efficiency of the carbon mineralisation in this system can be evaluated by the mineral sequences forming and their relative abundance, as described in section 4.1, and in Figs. 5, 7, and 8. Near the injection well, where the pH is low and the pCO_2 is high, the only phase calculated to be supersaturated is chalcedony (Table 4). At these conditions, the dissolution of the pre-existing phases occurs, leading to increased permeability and porosity near the injection well.

Further from the injection well, as the pH increases, the increased formation of secondary minerals occurs. The carbonation efficiency depends on the availability of the cations, mostly Ca, Mg, and Fe, provided by the dissolution of the primary rock, and the competition for these cations by other minerals such as zeolites and smectites – see section 4.1, and Fig. 7. Taking this into account, the most efficient carbonation during the second breakthrough occurred at pH ranging from ~5.2 to 6.5. At these conditions the only non-carbonate phases forming are chalcedony, and Al- and Fe-hydroxides (Fig. 5 and 7). No other secondary minerals compete for the available Ca-, Fe-, and Mg-cations liberated by the basalt dissolution, nor for the available pore space. We can refer to this as the "sweet-spot" of mineral carbonation in basalts at 20-50°C.

At lower CO_2 partial pressures, and higher pH, the formation of carbonate minerals is limited somewhat by the formation of zeolites and smectites, and other clay minerals. This can affect the efficiency of the carbon mineralisation dramatically, since these minerals consume both cations and pore space. Additionally, both zeolites and smectites are voluminous hydrated minerals. The net effect of these minerals on porosity is evident in Fig. 8, which illustrates the volume change of primary and secondary minerals along the reaction flow path.

Provided that the storage formation consists of relatively fresh, porous, and permeable basalts that respond to the injection by gradually increasing the injected fluid pH to conditions suitable for carbonate formation, the efficiency of the system is maximized by injecting at a rate fast enough to keep the pH low near the injection well. This prevents clogging by ensuring only minor local secondary mineral precipitation near the injection

well, and keeps the pCO_2 sufficiently high so that zeolites and clay formation only occurs at some distance from this well. This observation suggests the importance of continuous CO_2-charged water injection, thus avoiding pH fluctuations that favour zeolite and smectite precipitation near the injection well, which would clog pore space and diminish permeability – and thereby lower the efficiency of the injection (Fig.7c and Fig. 8).

However, as clearly seen in high-temperature geothermal fields, there are ways to preserve or recover permeability. Basaltic formations are mostly located in tectonically active areas, where faults and fractures are common and have large effect on the permeability (e.g. Fisher, 1998; Flóvenz and Saemundsson, 1993). Such is the case at the CarbFix site as demonstrated by the fracture flow of the first breakthrough. The injection of the CO_2-rich fluid can also cause hydrological fracturing due to overpressure and thermal cracking in areas of high geothermal gradient (e.g. Axelsson et al., 2006). Lastly, volume changes due to the precipitation of secondary minerals might also stimulate micro-fracturing of the host-rock. The permeability of basaltic rocks, nevertheless, naturally diminishes with increased age, due to progressive alteration, and gradual burial of the strata (e.g. Sigurdsson and Stefánsson, 1994).

The reaction path calculations define the amount of basaltic rocks required for mineralisation of the injected CO_2. For the second breakthrough, the dissolution of ~106 g of basaltic glass is required to dissolve into each kg of the injected fluid to mineralise about 95% of the injected carbon. This result indicates that about 500 tonnes of basaltic glass were dissolved in response to the 175 tonnes of CO_2 injected at the CarbFix-site in January 2012. Calculations suggests that this would result in the formation of approximately 420 tonnes of carbonates, about 450 tonnes of zeolites, and about 100 tonnes of smectites.

4.3 The effect of the presence of calcite in the original reservoir rock

The rapid dissolution rates of calcite in acidic fluids, if present in the original host rock, could play a significant role at the onset of the injection by raising the pH of the injected fluids via the reaction:

$$CaCO_3 + CO_2 + H_2O = Ca^{2+} + 2CO_3^{2-} + 2H^+ \leftrightarrow Ca^{2+} + 2HCO_3^-$$

The $^{14}C/^{12}C$ ratio of samples collected during the first breakthrough from the HN-04 monitoring well suggests a 50% dilution of the carbon in the fluid, and during the second breakthrough a 10% dilution, most likely via calcite dissolution at the onset of the injection (Matter et. al. 2016). The effect of this added calcite was evaluated by removing the dissolution of calcite pre-existing in the formation basalts from the previous calculations. The results of these calculations are summarized in Fig. 9b-c for the first breakthrough, and Fig. 10b-c, for the second breakthrough.

The effect of the addition of calcite to the system is twofold:

1) It affects the chemical composition of the carbonates forming, with more Ca rich carbonates calculated to form at earlier times due to the increased availability of Ca in the system (Figs.9-10 b-c).
2) It increases the rate of pH increase of the fluids following their injection (see Figs. 9-10 a). The more rapid pH increase leads to an earlier onset of carbonate mineral precipitation. Note, however, that kinetics are not considered in our modelling which could have a significant effect on these results.

In the absence of calcite dissolution, Mg-Fe-solid solutions are formed during the first breakthrough instead of Ca-Mg-Fe-solid solutions; and calcite does not reach saturation during the second breakthrough at pH <8. This could have an effect on the carbon mineralisation due to potential differences in precipitation rates, and stability of carbonates of different composition in the system.

4.4 The reactive surface area at the CarbFix site

The model calculations of the first and second breakthroughs described above provide estimates of the mass of basalt dissolved as the injected fluid moved from the injection to the first monitoring well. These masses can be used together with basalt dissolution rates

reported in the literature and PHREEQC to estimate the reactive surface area that interacted with the injected fluids during the two breakthroughs.
Such calculations yielded a reactive surface area of 0.4 m^2/kg water for the first breakthrough by taking account of the surface area normalized crystalline basalt dissolution rates reported by Gudbrandsson et al. (2011) and 13.6 m^2/kg water for the second breakthrough, taking account of the surface area basaltic glass dissolution rates reported by Oelkers and Gislason (2001). These estimates can be compared with the geometric surface areas calculated for idealised fractured or porous flow. Taking account of equations summarized by Oelkers (1996), the surface area of a 1 cm wide smooth fracture would be 0.2 m^2/kg water, whereas a 0.01 cm wide smooth fracture would be 20 m^2/kg water. Similarly a surface area of closed packed 1 cm diameter spheres would be 1.7 m^2/kg water, or 17 m^2/kg water for 0.1 cm diameter close packed spheres. The retrieved surface area of the CarbFix subsurface basalts is thus consistent with flow through fractured or pervasively porous basalt. Moreover, the relative reactive surface area determined for the first breakthrough was estimated to be 34 times smaller than that for the second breakthrough, consistent with the former fluid flowing though a wider more direct fracture network. The consistency of these field based surface area estimates with calculated geometric surface areas thus validates to some degree the model calculations described above.

5 Conclusions

Several major conclusions result from this study.

1. The mineralisation of the bulk of the CO_2 injected during the CarbFix project is driven by basaltic glass dissolution during the first ~400 days after the onset of its injection. This mineralization occurs during slow flow through porous basalts.
2. Considerable mineralisation appears to be driven by crystalline basalt dissolution along a faster fracture flow pathway. The crystalline basalts of the interiors of the lava pile are likely transected by fractures that hosts this flow path.
3. Even though the dissolution of the primary rocks is a contributor to the pH increase of the injected fluids, the mixing of the injected fluids with the formation waters also

contributes considerably to the pH increase. The pH of the injected fluids would have increased from 3.7 to 4.6 during the first breakthrough and from 3.7 to 4.1 during the second breakthrough, due to the non-reactive mixing of the injected acidic fluids with the more alkaline formation waters.

4. The efficiency of the carbon injection is limited by the permeability and/or porosity, and the availability of cations, both of which are limited by zeolite and smectite formation at higher pH and lower pCO_2. It is therefore essential to keep the pCO_2 high enough to prevent zeolites and clay formation near the injection well, but the pH high enough to be favour carbonate formation at a distance. The most efficient carbonate formation is computed to take place at pH from ~5.2 to 6.5. This pH favours carbonate precipitation due to the elevated pCO_2 of the system but avoids the precipitation of filling Al-silicates, and can be referred to as the "sweet-spot" of mineral carbonation in basalts at low temperature (20-50°C).
5. The mineralisation of ~95% of the 175 tonnes of CO_2 that were injected at the CarbFix-site in January 2012 would, according to the modelling calculations, require dissolution of about 500 tonnes of basaltic glass. This would result in the formation of about 420 tonnes of carbonates, 450 tonnes of zeolites, and about 100 tonnes of smectites.
6. Calcite dissolution taking place at the onset of the injection does not greatly affect chemical evolution of the system, though it influences which carbonates form and contributes to more rapid pH rise during the injection.

Acknowledgements

We acknowledge funding from the Environmental Fund of Reykjavik Energy; the European Commission through the projects CarbFix (EC coordinated action 283148), Min-GRO (MC-RTN-35488), Delta-Min (PITN-GA-2008-215360), and CO_2-REACT (EC Project 317235); the U.S. Department of Energy under award number DE-FE0004847; Nordic fund 11029-NORDICCS; and the Icelandic GEORG Geothermal Research fund (09-02-001).

We thank Edda Sif Aradóttir, Bergur Sigfússon, Ingvi Gunnarsson, Einar Gunnlaugsson and Hólmfríður Sigurðardóttir at Reykjavík Energy, Juerg Matter at the University of Southampton, Magnús Þór Arnarson at Mannvit Engineering, Guðni Axelsson at ISOR, Domenik Wolff-Boenisch at Curtin University in Australia, Helgi A. Alfreðsson at the University of Iceland and Martin Stute and Wallace S. Broecker at Columbia University for their contribution to the CarbFix project.

References

Alfredsson, H.A., Oelkers, E.H., Hardarsson, B.S., Franzson, H., Gunnlaugsson, E. and Gislason, S.R. (2013) The geology and water chemistry of the Hellisheidi, SW-Iceland carbon storage site. *Int. J. Greenh. Gas Control* **12**, *399-418.*

Appelo, C.A.J., Parkhurst, D.L. and Post, V.E.A. (2014) Equations for calculating hydrogeochemical reactions of minerals and gases such as CO_2 at high pressures and temperatures. *Geochim. Cosmochim. Acta* **125**, 49-67.

Aradóttir, E.S.P., Sonnenthal, E.L., Björnsson, G. and Jónsson, H. (2012) Multidimensional reactive transport modeling of CO_2 mineral sequestration in basalts at the Hellisheidi geothermal field, Iceland. *Int. J. Greenh. Gas Control* **9**, 24-40.

Axelsson, G., Þórhallson, S. and Björnsson, G. (2006) Stimulation of geothermal wells in basaltic rock in Iceland, ENGINE – ENhanced Geothermal Innovative Network for Europe, Workshop 3, "Stimulation of reservoir and microseismicity", Zürich, Switzerland.

Broecker, W. (2007) Climate change: CO_2 arithmetic. *Science* **315**, 1371.

Erbach, G. (2016) The Paris Agreement - A new framework for global climate action. European Parliamentary Research Service. European Parliament.

Fisher, A.T. (1998) Permeability within basaltic oceanic crust. *Rev. Geophys*. **36**, 143-182.

Flóvenz, Ó.G. and Saemundsson, K. (1993) Heat flow and geothermal processes in Iceland. *Tectonophysics* **225**, 123-138.

Franzson, H. (2000) Hydrothermal evolution of the Nesjavellir high-temperature system, Iceland, *Proceedings World Geothermal Congress*, Kyushu - Tohoku, Japan. P. 2075-2080.

Franzson, H., Zierenberg, R. and Schiffman, P. (2008) Chemical transport in geothermal systems in Iceland: Evidence from hydrothermal alteration. *J. Volcanol. Geotherm. Res.* **173**, 217-229.

Galeczka, I., Wolff-Boenisch, D., Oelkers, E.H. and Gislason, S.R. (2014) An experimental study of basaltic glass– H_2O– CO_2 interaction at 22 and 50°C: Implications for subsurface storage of CO_2. *Geochim. Cosmochim. Acta* **126**, 123-145.

Gislason, S.R., Broecker, W.S., Gunnlaugsson, E., Snæbjörnsdóttir, S.Ó., Mesfin, K.G., Alfredsson, H.A., Aradottir, E.S., Sigfusson, B., Gunnarsson, I., Stute, M., Matter, J.M., Arnarson, M.T., Galeczka, I.M., Guðbrandsson, S., Stockman, G., Wolff-Boenisch, D., Stefansson, A., Ragnheidardottir, E., Faathen, T., Gysi, A.P., Olssen, J., Didriksen, K., Stippe, S., Menez, B. and Oelkers, E.H. (2014) Rapid solubility and mineral storage of CO_2 in basalt. *Energy Procedia* **63**, 4561-4574.

Gislason, S.R. and Oelkers, E.H. (2003) Mechanism, rates, and consequences of basaltic glass dissolution: II. An experimental study of the dissolution rates of basaltic glass as a function of pH and temperature. *Geochim. Cosmochim. Acta* **67**, 3817-3832.

Gislason, S.R. and Oelkers, E.H. (2014) Carbon Storage in Basalt. *Science* **344**, 373-374.

Goldberg, D. and Slagle, A.L. (2009) A global assessment of deep-sea basalt sites for carbon sequestration. *Energy Procedia* **1**, 3675-3682.

Gudbrandsson, S., Wolff-Boenisch, D., Gislason, S.R. and Oelkers, E.H. (2011) An experimental study of crystalline basalt dissolution from $2 < pH < 11$ and temperatures from 5 to 75 °C. *Geochim. Cosmochim. Acta* **75**, 5496-5509.

Guy, C. and Schott, J. (1989) Multisite surface reaction versus transport control during the hydrolysis of a complex oxide. *Chem. Geol.* **78**, 181–204.

Gysi, A.P. and Stefánsson, A. (2011) CO_2–water–basalt interaction. Numerical simulation of low temperature CO_2 sequestration into basalts. *Geochim. Cosmochim. Acta* **75**, 4728-4751.

Gysi, A.P. and Stefánsson, A. (2012) CO_2-water–basalt interaction. Low temperature experiments and implications for CO_2 sequestration into basalts. *Geochim. Cosmochim. Acta* **81**, 129-152.

Helgadóttir, H.M. (2011) Stratigraphy and hydrothermal alteration of the Gráuhnúkar geothermal system in the southern part of the Hengill area. Master thesis from the University of Iceland p. 123.

Hoffert, M., Caldeira, K., Benford, G., Criswell, D., Green, C., Herzog, H., Jain, A., Kheshgi, H., Lackner, K., Lewis, J., Lightfood, H., Manheimer, W., Mankins, J., Mauel, M., Perkins, L., Schlesinger, M., Volk, T. and Wigley, T. (2002) Advanced technology paths to global climate stability: energy for a greenhouse planet. *Science* **298**.

IEA (2015) Energy Technology Perspectives 2015 - Mobilising Innovation To Accelerate Climate Action. International Energy Agency, Paris, France.

IEA (2016) World Energy Outlook 2016 - Executive summary. International Energy Agency, Paris, France.

IPCC (2014) Climate Change 2014: Mitigation of Climate Change. Contribution of Working Group III to the Fifth Assessment, in: Edenhofer, O., R. , Pichs-Madruga, r., Sokona, Y., Farahani, E., Kadner, S., Seyboth, K., Adler, A., Baum, I., Brunner, S., Eickemeier, P., Kriemann, B., Savolainen, J., Schlömer, S., von Stechow, C., Zwickel T., Minx, J.C. (Eds.). International Panel on Climate Change

Khalilabad, M.R., Axelsson, G. and Gislason, S.R. (2008) Aquifer characterization with tracer test technique; permanent CO_2 sequestration into basalt, SW Iceland. *Min. Mag*. **72**, 121-125.

Kloprogge, T., Komarneni, S. and Amonette, J.E. (1999) Synthesis of smectite clay minerals: A critical review. *Clays Clay miner.* 47, 529-554.

Kristmannsdóttir, H. and Tómasson, J. (1978) Zeolite zones in geothermal areas in Iceland. In Sand., L. B., and Mumpton, F. A., (eds.) *Natural Zeolites: Occurrence, Properties, Use.* 277-284. Elmsford, New York, Pergamon Press,

Lackner, K. (2003) A guide to CO_2 sequestration. *Science* **300**, 1677–1678.

Matter, J.M., Stute, M., Snæbjörnsdóttir, S.Ó., Oelkers, E.H., Gislason, S.R., Aradottir, E.S., Sigfusson, B., Gunnarsson, I., Sigurdardottir, H., Gunnlaugsson, E., Axelsson, G., Alfredsson, H.A., Wolff-Boenisch, D., Mesfin, K., Fernandez de la Reguera Taya, D., Hall, J., Dideriksen, K. and Broecker, W.S. (2016) Rapid carbon mineralization for permanent and safe disposal of anthropogenic carbon dioxide emissions. *Science* **352**, 1312-1314.

McGrail, B.P., Schaef, H.T., Ho, A.M., Chien, Y.-J., Dooley, J.J. and Davidson, C.L. (2006) Potential for carbon dioxide sequestration in flood basalts. *J. Geophys. Res. Sol. Earth* **(111)**.

Neuhoff, P.S., Fridriksson, T. and Armannsson, H. (2008) Porosity evolution and mineral paragenesis during low-grade metamorphism of basaltic lavas at Teigarhorn, Eastern Iceland. *Am. J. Sci.* **299**, 467-501.

Neuhoff, P.S., Fridriksson, T. and Bird, D.K. (2000) Zeolite Parageneses in the North Atlantic Igneous Province: Implications for Geotectonics and Groundwater Quality of Basaltic Crust. *Int. Geol. Rev.* **42,** 15-44.

Neuhoff, P.S., Th., F., Arnorsson, S. and Bird, D.K. (1999) Porosity evolution and mineral paragenesis during low-grade metamorphism of basaltic lavas at Teigarhorn, Eastern Iceland. *Am. J. Sci.* **299**, 467-501.

OECD/IEA (2016) Enhancing transparency of climate change mitigation under the Paris agreement: Lessons from experience, in: Briner, G., Moarif, S. (Eds.). OECD/IEA, Paris, France.

Oelkers E.H. (1996) The physical and chemical properties of rocks and fluids for chemical mass transport calculations. *Rev. Min.* **34,** 131-191.

Oelkers, E. H. and Schott, J. (2005) Geochemical aspects of CO_2 sequestration. *Chem. Geol.***217**, 183–186.

Oelkers, E.H. and Gislason, S.R. (2001) The mechanism, rates and consequences of basaltic glass dissolution: I. An experimental study of the dissolution rates of basaltic glass as a function of aqueous Al, Si and oxalic acid concentration at 25°C and pH = 3 and 11. *Geochim. Cosmochim. Acta* **65**, 3671-3681.

Pacala, S. and Socolow, R. (2004) Stabilization wedges: solving the climate problem for the next 50 years with current technologies. *Science* **305**, 968-972.

Parkhurst, D.L. and Appelo, C.A.J. (2013) Description of input and examples for PHREEQC version 3—A computer program for speciation, batch-reaction, one-dimensional transport, and inverse geochemical calculations. US Geological Survey.

Richter, B., Guðlaugsson, S.Þ., Steingrímsson, B., Björnsson, G., Bjarnason, J.Ö. and Þórhallson, S. (1999) Svartsengi well SJ-18: Drilling, research and production (in Icelandic). National Energy Authority of Iceland, OS-99117.

Rogers, K.L., Neuhoff, P.S., Pedersen, A.K. and Bird, D.K. (2006) CO_2 metasomatism in a basalt-hosted petroleum reservoir, Nuussuaq, West Greenland. *Lithos* **92**, 55-82.

Schiffman, P. and Fridleifsson, G.O. (1991) The smectite-chlorite transition in drillhole NJ-15, Nesjavellir Geothermal Field, Iceland: XRD, BSE and electron microprobe investigations. *J. Metamorph Geol.* **9**, 679-696.

Sigfusson, B., Gislason, S.R., Matter, J.M., Stute, M., Gunnlaugsson, E., Gunnarsson, I., Aradottir, E.S., Sigurdardottir, H., Mesfin, K.G., Alfredsson, H.A., Wolff-Boenisch, D., Arnarson, M.T. and Oelkers, E.H. (2015) Solving the carbon-dioxide buoyancy challenge: The design and field testing of a dissolved CO_2 injection system. *Int. J. Greenhouse Gas Control* **37**, 213-219.

Snæbjörnsdóttir, S.Ó. (2011) The Geology and Hydrothermal Alteration at the Western Margin of the Hengill Volcanic System (Master thesis, in Icelandic), Institute of Earth Sciences. University of Iceland, Reykjavik, p. 263.

Snæbjörnsdóttir, S.Ó., Oelkers, E.H., Mesfin, K., Aradóttir, E.S., Dideriksen, K., Gunnarsson, I., Gunnlaugsson, E., Matter, J.M., Stute, M. and Gislason, S.R. (2017) The chemistry and saturation states of subsurface fluids during the in situ mineralisation of CO_2 and H_2S at the CarbFix site in SW-Iceland. *Int. J. Greenh. Gas Control* **58**, 87-102.

Snæbjörnsdóttir, S.Ó., Wiese, F., Fridriksson, T., Ármannsson, H., Einarsson, G.M. and Gislason, S.R. (2014) CO_2 storage potential of basaltic rocks in Iceland and the oceanic ridges. *Energy Procedia* **63**, 4585-4600.

Stefansson, V., Sigurdsson, O., Gudmundsson, A., Franzson, H., Fridleifsson, G. O., Tulinius, H. (1997) Core measurements and Geothermal Modelling. Second Nordic Symposium on Petrophysics: Fractured reservoir. Nordic petroleum series (1), p. 198-220

Stockmann, G.J., Wolff-Boenisch, D., Gislason, S.R. and Oelkers, E.H. (2011) Do carbonate precipitates affect dissolution kinetics? 1: Basaltic glass. *Chem. Geol.* **284**, 306-316.

UN (2015a) United Nations/ Framework Convention on Climate Change. Adoption of the Paris Agreement, 21st Conference of the Parties, Paris.

UN (2015b) The Paris Agreement. Report of the Conference of the Parties on its twenty-first session, held in Paris from 30 November to 13 December 2015.

Wolff-Boenisch, D., Gislason, S.R., Oelkers, E.H. and Putnis, C.V. (2004) The dissolution rates of natural glasses as a function of their composition at pH 4 and 10.6, and temperatures from 25 to 74°C. *Geochim. Cosmochim. Acta* **68**, 4843-4858.

Yann, R.d.P., Jeffery, M.L., Gutschow, J., Rogelj, J., Christoff, P. and Meinshausen, M. (2017) Equitable mitigation to achieve the Paris Agreement goals. *Nature Clim. Change* **7**, 38-43.

Tables

Table 1. Secondary phases identified in drill cuttings in the top 1000 m of the injection well, HN-02 (Alfredsson et al., 2013; Helgadóttir, 2011). The total depth of the well is 2001 m. The depth of the target storage formation is ~400-800 m (e.g. Alfredsson et al., 2013; Aradóttir et al., 2012).

	Chemical composition	**Depth of appearance**
Zeolites		
Thomsonite	$NaCa_2Al_5Si_5O_{10}\cdot 6H_2O$	250-650
Chabazite	$NaCa_2Al_5Si_{13}O_{36}\cdot 14H_2O$	250-760
Analcime	$NaAlSi_2O_6\cdot H_2O$	250-*1000*
Mesolite	$Na_2Ca_2Al_6Si_9O_{30}\cdot 8H_2O$	600-*1000*
Scolecite	$CaAl_2Si_3O_{10}\cdot 3H_2O$	220-*1000*
Heulandite	$NaCa_4(Al_9Si_{27}O_{72})\cdot 28H_2O$	480-*1000*
Stilbite	$(Ca,Na)_{2-3}Al_3(Al,Si)2Si_{13}O_{36}\cdot 12H_2O$	820-*1000*
Carbonates		
Aragonite	Ca_8CO_3	150-500
Calcite	Ca_8CO_3	500-*1000*
Dogtooth calcite	Ca_8CO_3	180-*1000*
Other Minerals		
Chalcedony	SiO_4	500-*1000*
Smectite (saponite)	$Ca_{0.1}Na_{0.1}Mg_{2.25}Fe^{2+}_{0.75}Si_3AlO_{10}(OH)_2\cdot 4(H_2O)$	200-*1000*

Table 2. The dissolution reactions for primary and secondary minerals included in the reaction path calculations and the logarithm of their equilibrium constants at 35 ^{o}C.

Mineral	Reaction	Logarithm of Equilibrium constants (Log K at 35 ^{o}C
Primary minerals/glasses		
Stapafell basaltic glass[1)]	$SiTi_{0.024}Al_{0.358}Fe_{0.188}Mg_{0.281}Ca_{0.264}Na_{0.079}K_{0.008}O_{3.370} + 2.644H^{+} + 0.726H_2O$ $= 0.358Al^{+3} + 0.264Ca^{+2} + 0.171Fe^{+2} + 0.017Fe^{+3} + H_4SiO_4 + 0.008K^{+} + 0.281Mg^{+2} + 0.079Na^{+} + 0.024Ti(OH)_4$	-0.07
Crystalline basalt[2)]:		
Plagioclase (An_{70})[1)] *44vol%; 30mol%*	$Ca_{0.7}Na_{0.3}Al_{1.7}Si_{2.3}O_8 + 8H_2O = 1.7Al(OH)_4^{-} + 0.7Ca^{+2} + 2.3H_4SiO_4 + 0.3Na^{+}$	-18.56
Olivine ($Fo_{43}Fa_{57}$)[1)] *17 vol%; 28mol%*	$(Mg_{0.43}Fe_{0.57})2SiO_4 + 4H+ = 1.14Fe^{+2} + H_4SiO_4 + 0.86Mg^{+2}$	22.29
Clinopyroxene[1)] *39 vol%; 42 mol%*	$Ca_{0.7}Mg_{0.84}Fe_{0.46}(SiO_3)_2 + 4H^{+} + 2H_2O = 0.7Ca^{+2} + 0.46Fe^{+2} + 2H_4SiO_4 + 0.84Mg^{+2}$	8.91
Secondary minerals		
Carbonates		
Calcite[3)]	$CaCO_3 + H^{+} = Ca^{2+} + HCO_3^{-}$	-8.54
Aragonite[3)]	$CaCO_3 + H^{+} = Ca^{2+} + HCO_3^{-}$	-8.41
Siderite[4)]	$FeCO_3 + H^{+} = Fe^{2+} + HCO_3^{-}$	-0.94
$Ca_{0.25}Mg_{0.50}Fe_{0.25}$ carbonate [4)]	$Ca_{0.25}Mg_{0.50}Fe_{0.25}CO_3 + H^{+} = 0.25Ca^{+2} + 0.5Mg^{+2} + 0.25Fe^{+2} + HCO_3^{-}$	0.77
$Mg_{0.25}Fe_{0.75}$ carbonate[4)]	$Mg_{0.25}Fe_{0.75}CO_3 + H^{+} = 0.75Fe^{+2} + 0.25Mg^{+2} + HCO_3^{-}$	-0.44
$Mg_{0.50}Fe_{0.50}$ carbonate[4)]	$Mg_{0.50}Fe_{0.50}CO_3 + H^{+} = 0.50Fe^{+2} + 0.50Mg^{+2} + HCO_3^{-}$	0.25
$Mg_{0.75}Fe_{0.25}$ carbonate[4)]	$Mg_{0.75}Fe_{0.25}CO_3 + H^{+} = 0.25Fe^{+2} + 0.75Mg^{+2} + HCO_3^{-}$	1.05
Zeolites		

Analcime [4)]	$Na_{0.96}Al_{0.96}Si_{2.04}O_6H_2O + 5H_2O = 0.96Al(OH)4^- + 2.04H_4SiO_4 + 0.96Na^+$	-15.10
Chabazite [4)]	$CaAl_2Si_4O_{12}{:}6H_2O + 6H_2O = 2Al(OH)_4^- + Ca^{+2} + 4H_4SiO_4$	-30.11
Thomsonite [4)]	$Ca_2NaAl_5Si_5O_{20}{:}6H_2O + 14H_2O = 5Al(OH)_4^- + 2Ca^{+2} + 5H_4SiO_4 + Na^+$	-59.54
Silica polymorphs		
Chalcedony [4)]	$SiO_2 + 2H_2O = H_4SiO_4$	-3.46
Clay minerals		
Mg-clay [a)]	$Ca_{0.04}Mg_{3.01}Al_{0.1}Si_{3.9}O_{10}(OH)_2 + 6H^+ + 4H_2O = 0.1Al(OH)_4^- + 0.04Ca^{+2} + 3.9H_4SiO_4 + 3.01Mg^{+2}$	19.31
Smectite[b), 4)]	$K_{0.03}Na_{0.05}Ca_{0.13}Mg_{0.81}Fe_{0.71}Al_{0.98}Si_{3.92}O_{10}(OH)_2 + 2.4H^+ + 7.6H_2O$ $= 0.98Al(OH)_4^- + 0.13Ca^{+2} + 0.71Fe^{+2} + 3.92H_4SiO_4 + 0.03K^+ + 0.81Mg^{+2} + 0.05Na^+$	-10.44
Smectite[c), 4)]	$K_{0.01}Na_{0.02}Ca_{0.25}Mg_{2.16}Fe_{0.78}Al_{0.77}Si_{3.32}O_{10}(OH)_2 + 5.64H^+ + 4.36H_2O$ $= 0.77Al(OH)_4^- + 0.25Ca^{+2} + 0.78Fe^{+2} + 3.32H_4SiO_4 + 0.01K^+ + 2.16Mg^{+2} + 0.02Na^+$	12.21
Smectite[d), 4)]	$K_{0.02}Na_{0.10}Ca_{0.26}Mg_{1.27}Fe_{1.91}Al_{01.08}Si_{2.94}O_{10}(OH)_2 + 5.92H^+ + 4.08H_2O$ $= 1.08Al(OH)_4^- + 0.26Ca^{+2} + 1.91Fe^{+2} + 2.94H_4SiO_4 + 0.02K^+ + 1.27Mg^{+2} + 0.01Na^+$	8.47
Smectite[e), 4)]	$K_{0.05}Na_{0.03}Ca_{0.18}Mg_{1.41}Fe_{1.78}Al_{1.02}Si_{3.03}O_{10}(OH)_2 + 5.8H^+ + 4.2H_2O$ $= 1.02Al(OH)_4^- + 0.18Ca^{+2} + 1.78Fe^{+2} + 3.03H_4SiO_4 + 0.05K^+ + 1.41Mg^{+2} + 0.03Na^+$	7.89
Ca-Saponite	$Ca_{0.165}Mg_3Al_{0.33}Si_{3.67}O_{10}(OH)_2 + 6H^+ + 4H_2O = 0.33Al(OH)_4^- + 0.165Ca^{+2} + 3.67H_4SiO_4 + 3Mg^{+2}$	20.42
Al- and Fe-hydroxides		
$Al(OH)_3$ amorph	$Al(OH)_3 + 3H^+ = Al^{3+} + 3H_2O$	1.10
Gibbsite (mircrocrystalline)	$Al(OH)_3 + H_2O = AlOH_4^- + H^+$	8.40
$Fe(OH)_3$ amorph	$Fe(OH)_3 + 3H^+ = Fe^{3+} + 3H_2O$	4.89

1) Dissolution reactions and solubility constants from Stefansson et al., 2001.
2) Modal abundances from Gudbrandsson et al. (2011)
3) Dissolution reactions and solubility constants from Parkhurst and Appelo, 2013.
4 Dissolution reactions and solubility constants from Gysi and Stefansson, 2011.

a) Natural clay mixtures from Crovisier et al. (1992
b) Natural di-/tri-octahedral smectite from Rogers et al. (2006)
c) Natural di-/tri-octahedral smectite from Rogers et al. (2006)
d) Natural di-/tri-octahedral smectite from Neuhoff et al. (2006)
e) Natural clay mixtures from Neuhoff et al. (1999)

Table 3. The measured and calculated chemical compositions of water samples collected from wells HN-01 and HN-04, and used in the geochemical calculations presented in this study.

Well	**HN-04**	**HN-01**	**HN-04**	**HN-04**
Sample representation (in model)	Background waters	Injected fluid after CO_2 dissolution	First breakthrough	Second breakthrough
Date	25.1.2012	3.2.2012	26.3.2012	3.4.2013
Sample ID	12KGM01	12KGM06	12KGM33	13SOS06
pH	9.2	3.7*	6.7	8.2
T (°C)	35	35	35	35
Alk. (meq/kg)	1.87	2.0	2.93	2.87
DIC (mmol/kg)	1.55	820*	4.00	2.83
Si (mmol/kg)	0.39	0.59	0.392	0.41
Ca (mmol/kg)	0.052	0.13	0.41	0.24
Mg (mmol/kg)	0.005	0.16	0.100	0.200
Na (mmol/kg)	2.18	2.04	2.37	2.73
K (mmol/kg)	0.018	0.024	0.021	0.024
Fe (µmol/kg)	0.061	0.021	20.0	0.184
Al (µmol/kg)	2.08	1.19	1.01	1.90

** Calculated value based on dissolution of 0.82 moles CO_2 per kg of the injected solution*

Table 4. The calculated saturation indices of the primary and secondary phases considered in this study (Table 2) in the sampled fluids described in Table 3.

	HN-04 Background waters	HN-01 Injected fluid after CO_2 dissolution	HN-04 First breakthrough	HN-04 Second breakthrough
pH	9.24	3.72	6.70	8.20
Stapafell basaltic glass	-1.86	-3.42	-1.10	-1.38
Plagioclase (An_{70})	-3.24	-20.75	-3.51	-2.49
Olivine ($Fo_{43}Fa_{57}$)	-5.83	-22.15	-8.06	-9.14
Clinopyroxene	8.29	-9.81	2.88	6.00
Calcite	0.17	-4.67	-1.10	0.13
Aragonite	0.03	-4.80	-1.24	-0.01
Siderite	-3.47	-5.19	0.15	-4.81
$Ca_{0.25}Mg_{0.50}Fe_{0.25}$-carbonate	-0.95	-4.47	-0.81	-0.86
$Mg_{0.25}Fe_{0.75}$-carbonate	-2.64	-4.87	-0.15	-3.43
$Mg_{0.50}Fe_{0.50}$-carbonate	-2.00	-4.74	-0.64	-2.23
$Mg_{0.75}Fe_{0.25}$-carbonate	-1.48	-4.73	-1.25	-1.16
Analcime	-0.26	-10.09	-0.66	0.07
Analcime_0.96	-0.20	-10.03	-0.60	0.13
Chabazite	0.03	-20.07	0.04	1.19
Thomsonite	1.62	-50.57	0.52	3.54
Chalcedony	-0.09	0.27	0.05	0.06
Smectite[b)]	0.20	-18.56	-0.73	-0.80
Smectite[c)]	2.33	-29.84	-4.46	0.10
Smectite[d)]	0.64	-33.94	-1.72	-4.06
Smectite[e)]	1.20	-32.31	-1.45	-3.11
Mg-Clay	4.00	-24.17	-6.74	3.22
Ca-Saponite	4.10	-26.63	-6.74	3.35
$Fe(OH)_{3(a)}$	-0.49	-3.85	1.39	0.93
$Al(OH)_{3(a)}$	-2.71	-8.17	-0.92	-1.73
Gibbsite (microcrystalline)	-0.94	-6.40	0.85	0.03

Figures

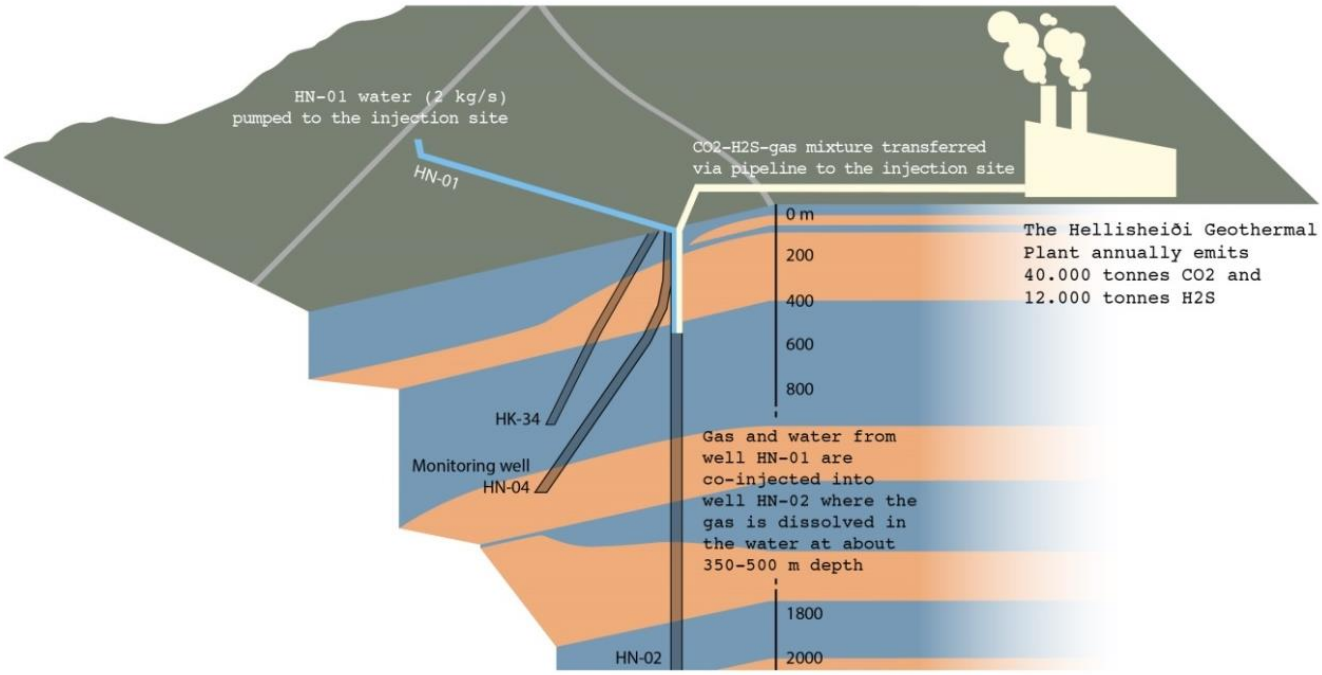

Fig. 1. Overview of the injection site at Hellisheidi, showing the infrastructure and the geological cross-section of the CarbFix injection site. Blue indicates lava flows and brown indicates hyaloclastic (glassy) formations. Modified from Alfredsson et al. (2013) and Snæbjörnsdóttir et al. (2017). The HN-01 water was co-injected into well HN-02 at a rate of 2 kg s^{-1} with the CO_2, which dissolves into the HN-02 water during injection. 1 kg s^{-1} of water was produced out of the first monitoring well HN-04 during, and after the injection to promote subsurface fluid flow.

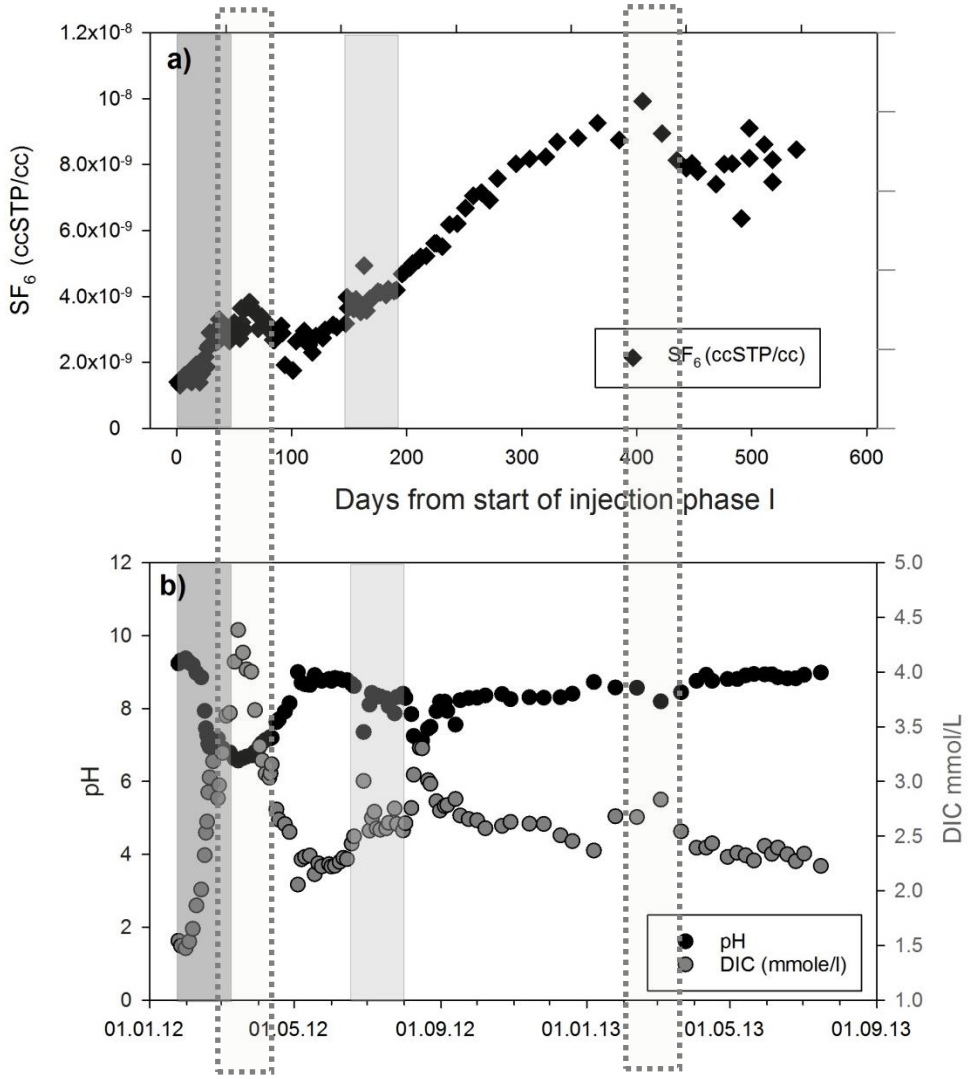

Fig. 2. Time evolution of the SF_6 tracer concentration (a) and the pH and DIC concentrations (b) in the first monitoring well (HN-04) during and after the injection. The period of the pure CO_2 injection is shaded (dark grey). A second injection of 73 tonnes of 75%CO_2-25%H_2S gas mixture is also shaded (light grey); the fate of this latter injection is not considered in this study. The two superimposed dotted columns frame represents the timing of the first and second breakthrough of the pure CO_2 injected fluid represented by the recovery of the SF_6 non-reactive tracer. The first breakthrough indicates a small aquifer, either a thin inter-layer or a fracture connecting the wells at shallow depth, rapidly channelling about ~3% of the injected solution. The second and main breakthrough is believed to be caused by flow through a much larger channel, characterised by homogeneous porous media flow with considerable dispersion and diffusion, as described in

detail by Khalibad et al. (2008).

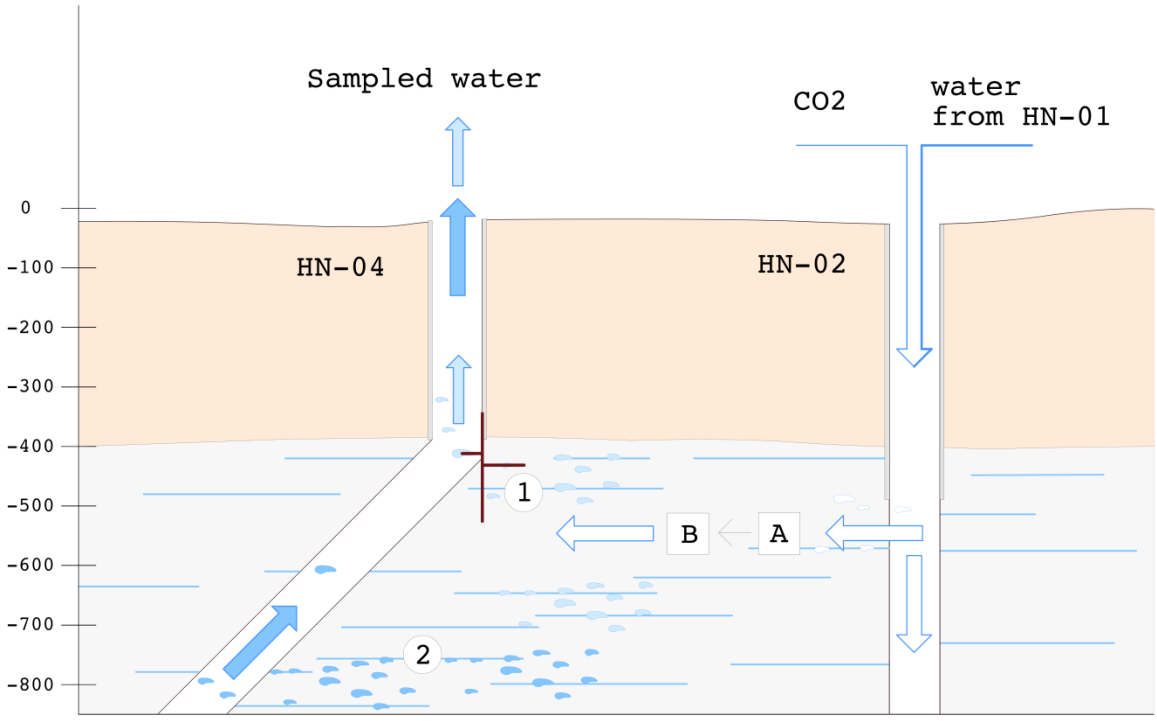

Fig. 3. Schematic illustration of the two breakthroughs considered on this study. Geochemical modelling in this study was done in two steps. A) The solid phases (crystalline basalt and calcite for the first breakthrough, basaltic glass for the second breakthrough) are dissolved into the injected fluid. B) The resulting fluid is mixed into the background waters in the ratio determined by the SF_6 non-reactive tracer concentration of the sampled fluids. This approach was adopted for both of the two breakthroughs, the first breakthrough characterized by a fast fracture flow (1) and the second and main breakthrough characterized by slower porous rock flow (2).

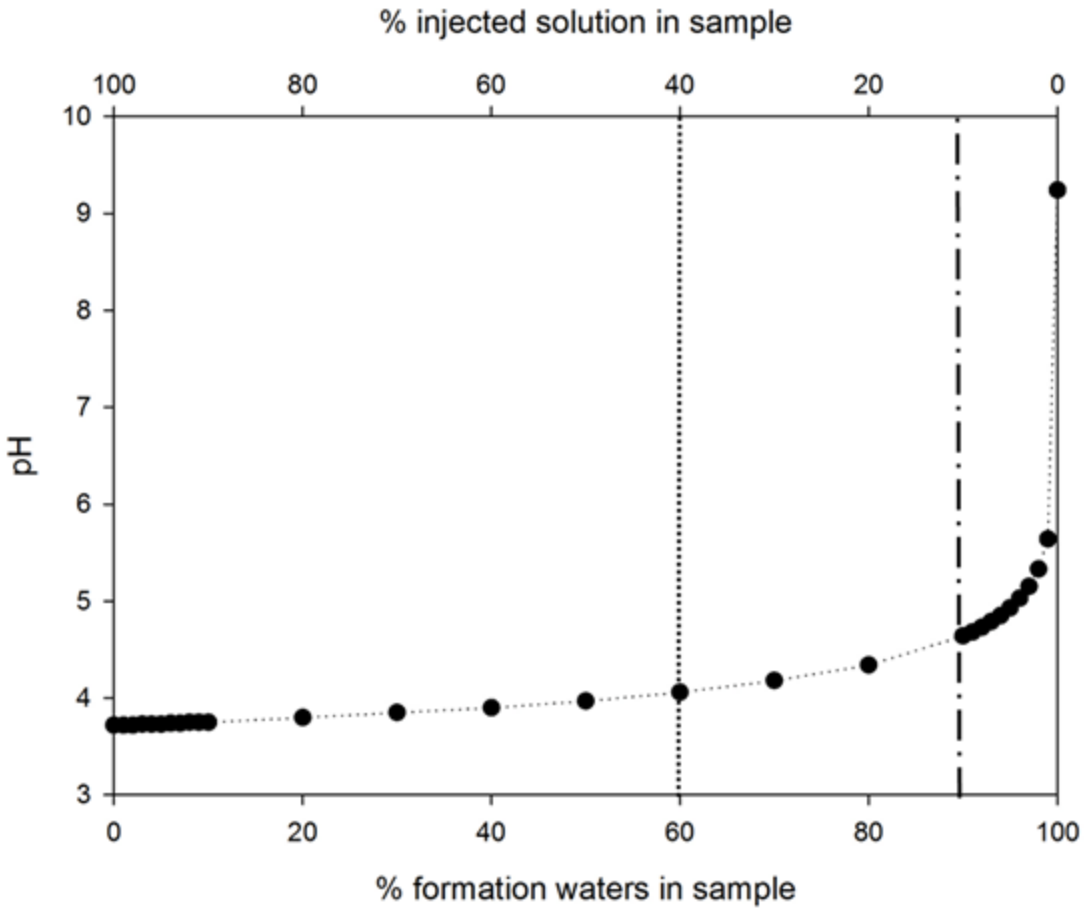

Fig. 4. Calculated effect of mixing the injected CO_2-charged fluid with the formation waters on the pH of the mixed fluid. The mixing fraction of the sample representing the first breakthrough (pH 4.6, 90% background water) is shown with a dashed-dotted line, and the mixing fraction of the sample representing the second breakthrough (pH 4.1, 60% background water) is presented as a dotted line.

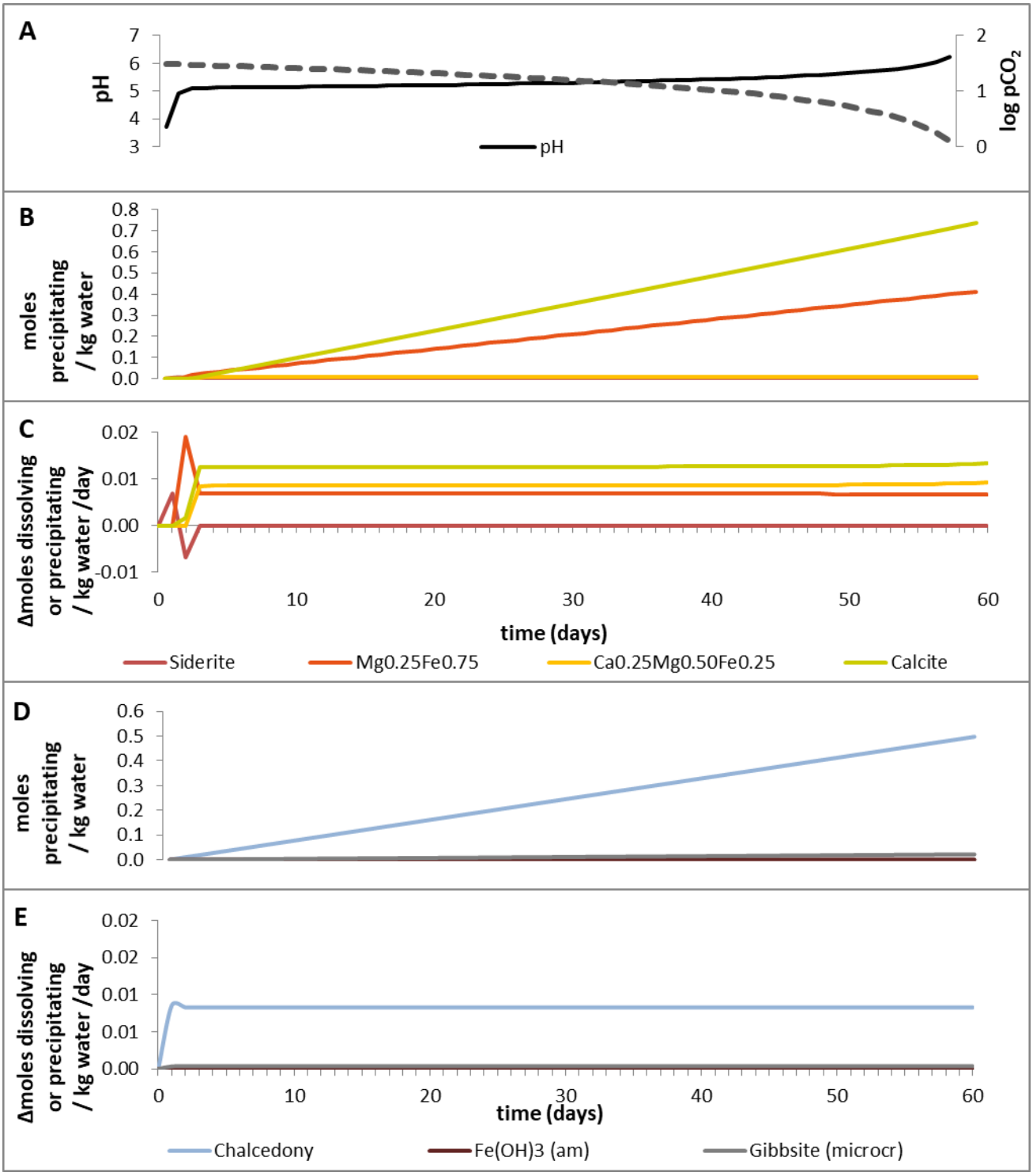

Fig. 5. Results for reaction path calculations at 35°C simulating the first breakthrough of the injected solution from the CO_2 injection at Hellisheidi in 2012. Progressive dissolution of a crystalline basalt consisting of 28 mol% olivine ($Fo_{43}Fa_{57}$), 42 mol% clinopyroxene, and 28

mol% plagioclase ($An_{70}Ab_{30}$) into the CO_2-charged injection fluid as prescribed using dissolution rates reported by Gudbrandsson et al. (2011) and 0.82 moles of calcite. a) The evolution of pH and pCO_2 during the reaction progress; b) total moles of carbonate minerals precipitated along the reaction path from each kg of injected CO_2-charged fluid; c) incremental number of moles of carbonate minerals dissolving or precipitating in each kg of water per day over the flow path (Δ moles); d) moles of non-carbonate minerals precipitated along the reaction path from each kg of injected CO_2-charged fluid; e) Δmoles of non-carbonate minerals dissolving or precipitating in each kg of water during the reaction process.

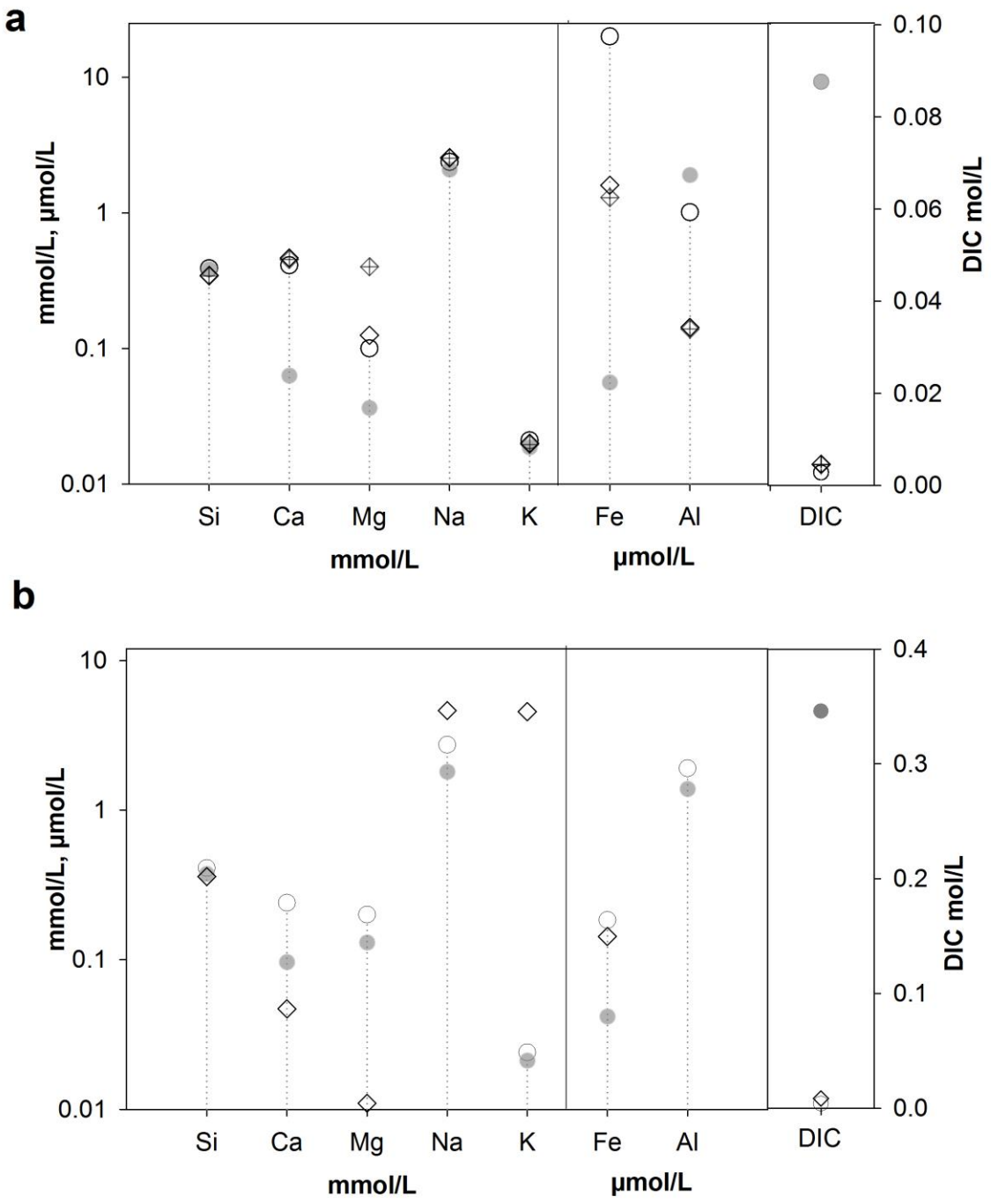

Fig. 6. Chemical composition of the sampled fluids, modelled fluids, and fluids after non-reactive mechanical mixing of the injected solution with the formation waters; a) the first breakthrough. The chemical composition of sample 12KGM33 is represented by circles and dotted lines, mechanical mixing (0.1:0.9) is represented by grey dots, modelled fluid composition

taking account of both crystalline basalt and calcite dissolution is represented by crossed diamonds, and modelled fluid compositions taking account of crystalline basalt dissolution, but excluding calcite dissolution is represented by empty diamonds; b) the second breakthrough. The chemical composition of sample 13SOS06 is represented by empty circles and dotted lines, mechanical mixing (0.4:0.6) is represented by grey dots, and modelled fluid composition using basaltic glass is represented by diamonds.

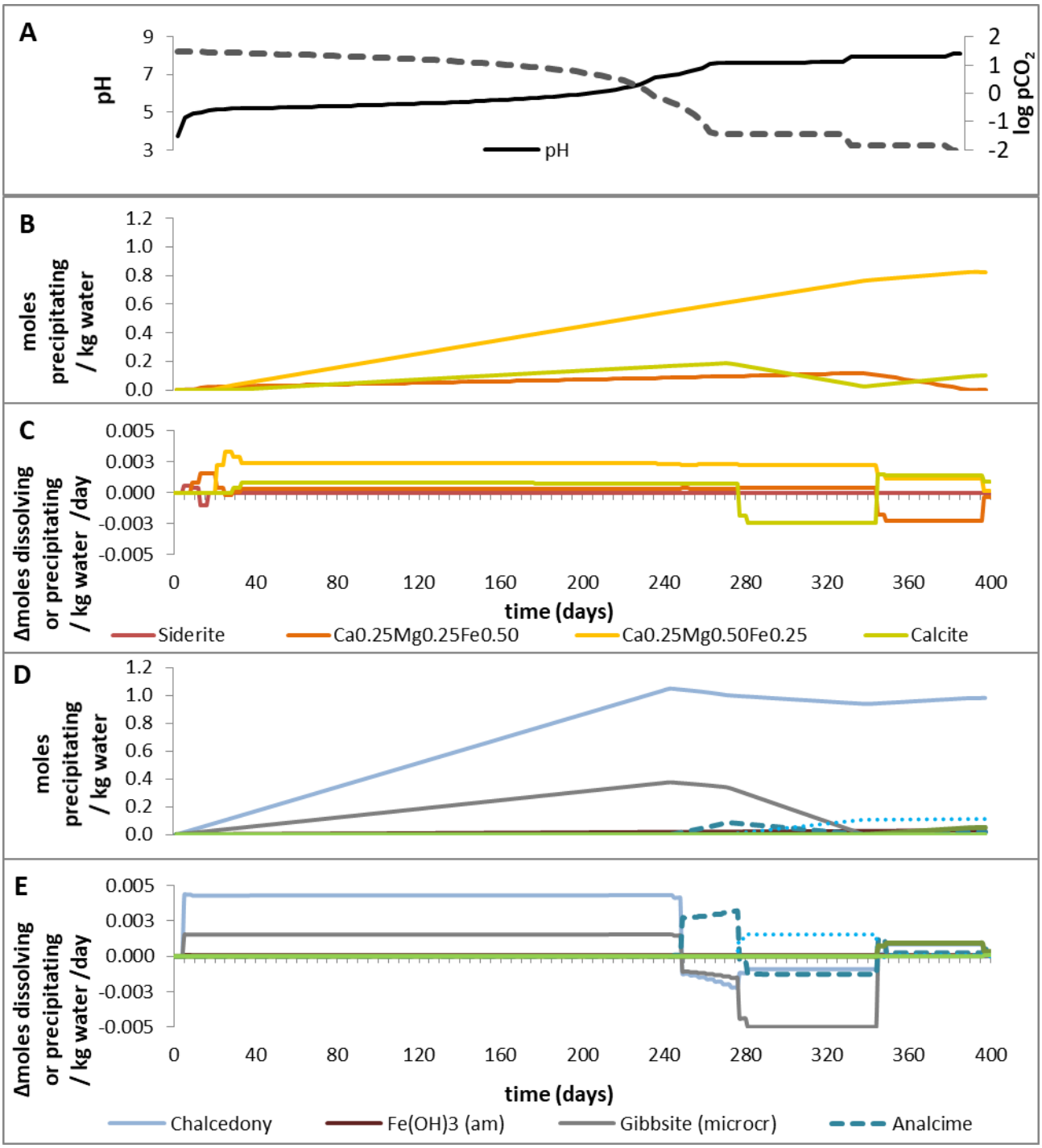

Fig. 7. Results for reaction path calculations at 35°C simulating the second breakthrough of the injected CO_2-charged fluid at Hellisheidi in 2012. Progressive dissolution of 0.86 moles basaltic glass into each kg of injected CO_2-charged fluid occurred over 400 days. a) The evolution of pH and pCO_2 during the basaltic glass dissolution; b) total number of moles of carbonates precipitated along the flow path from each kg of injected CO_2-charged fluid; c) incremental

number of moles of carbonate minerals dissolving or precipitating in each kg of water per day during the reaction path; d) total moles of non-carbonate secondary minerals precipitated along the reaction path from each kg of injected CO_2-charged fluid, and e) incremental number of moles of non-carbonate minerals dissolving or precipitating in each kg of water each day during the reaction process.

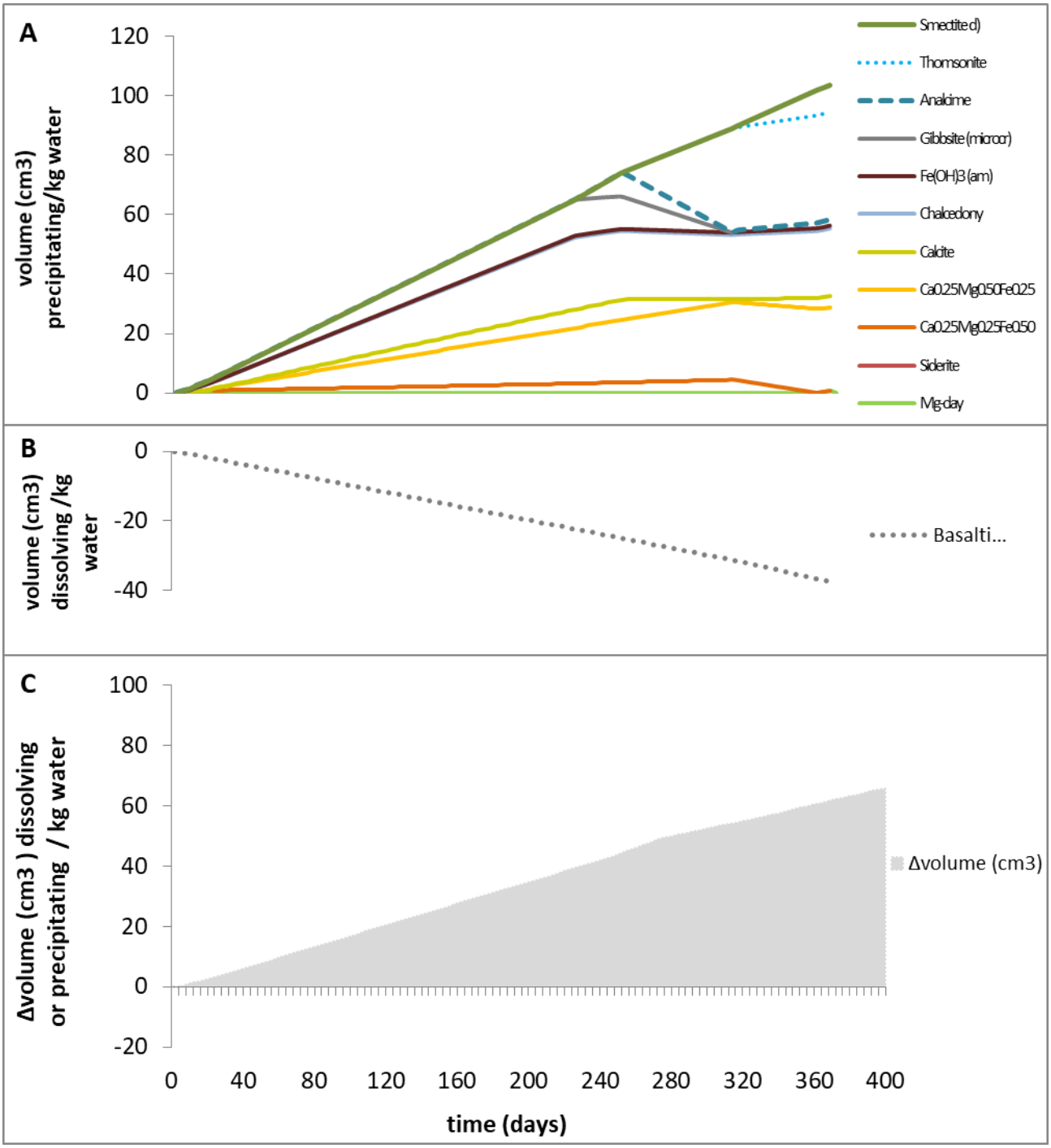
A
volume (cm3) precipitating/kg water
120
100
80
60
40
20
0
Smectite(d)
Thomsonite
Analcime
Gibbsite(microcr)
Fe(OH)3(am)
Chalcedony
Calcite
Ca0.25Mg0.50Fe0.25
Ca0.25Mg0.25Fe0.50
Siderite
Mg-clay
B
volume (cm3) dissolving /kg water
0
-20
-40
Basalti...
C
Δvolume (cm3) dissolving or precipitating / kg water
100
80
60
40
20
0
-20
0
40
80
120
160
200
240
280
320
360
400
time (days)
Δvolume (cm3)

Fig. 8. Results for reaction path calculations at 35°C simulating the second breakthrough of the injected CO_2-charged fluid at Hellisheidi in 2012. This simulation took account to the progressive dissolution of 0.86 moles basaltic glass into each kg of injected CO_2-charged fluid along the flow path. a) Volumes of secondary phases precipitating along the reaction path, b) volume of basaltic glass dissolving along the reaction path, and c) the volume change (Δ volume) due to dissolution of primary basaltic glass, and precipitation of secondary phases along the flow path.

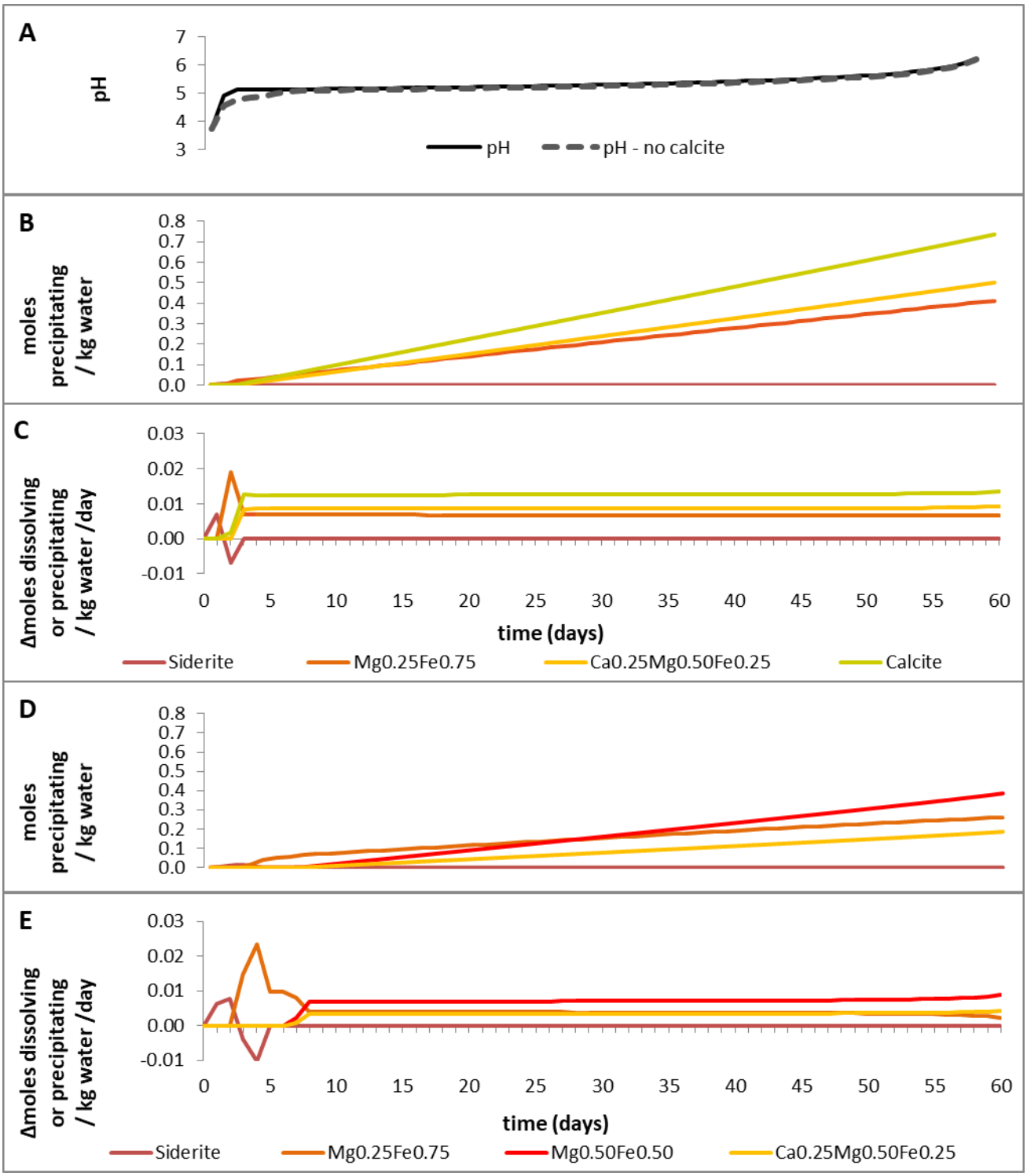

Fig. 9. Results for reaction path calculations simulating the effect of calcite dissolution during the first breakthrough on a) the evolution of pH for the calculations with calcite dissolution (solid line), and in the absence of calcite dissolution (broken line); b) the total mass of carbonate minerals precipitated along the reaction path from each kg of injected CO_2-charged fluid with

calcite dissolution considered (as depicted in fig. 5 b); c) The incremental number of moles of carbonate minerals dissolving or precipitating in each kg of water per day during the reaction process with calcite dissolution considered (as depicted in fig. 5 c); d) the total mass of carbonate minerals precipitated along the reaction path from each kg of injected CO_2-charged fluid with calcite dissolution excluded; e) the incremental number of moles of carbonate minerals dissolving or precipitating in each kg of water per day during the reaction process with calcite dissolution excluded.

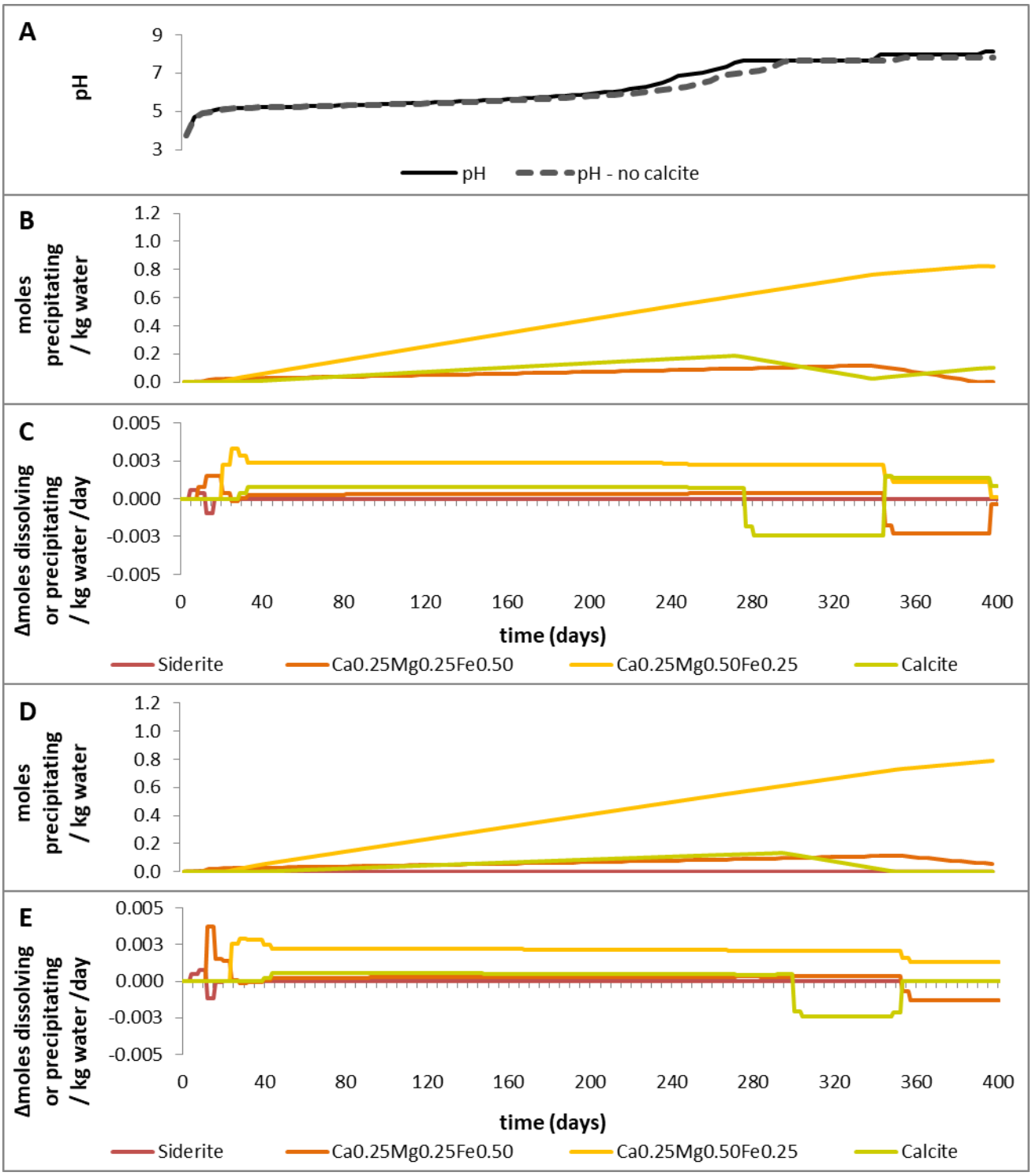

Fig. 10. Results for reaction path calculations simulating the effect of calcite dissolution during the second breakthrough on a) the evolution of pH for the calculations with calcite dissolution (solid line), and in the absence of calcite dissolution (broken line); b) the total mass of carbonate minerals precipitated along the reaction path from each kg of injected CO_2-charged fluid with

calcite dissolution considered (as depicted in fig. 5 b); c) the incremental number of moles of carbonate minerals dissolving or precipitating in each kg of water per day during the reaction process with calcite dissolution considered (as depicted in fig. 5 c); d) the total mass of carbonate minerals precipitated along the reaction path from each kg of injected CO_2-charged fluid with calcite dissolution excluded; e) the incremental number of moles of carbonate minerals dissolving or precipitating in each kg of water per day during the reaction process with calcite dissolution excluded.